Jour. Sci. Hiroshima Univ., Ser. C, Vol. 10, No. 1, 87–118 (1994)

Mineralogical Study of Landslide in Monden Area, Southwest Okayama Prefecture, Japan

By
Pucai YANG

with 7 Tables, 40 Text-figures and 9 Plates

(received, June 29, 1994)

Abstract: Landslides, occurring in Tertiary Nyokan formation of the Monden area, at the southwestern part of Okayama Prefecture, southwest Japan were investigated to clarify the occurrence mechanism of Tertiary mudstone landslide from mineralogical viewpoint. The landslide of the area is characterized by slow creep movement at the rate of 2 to 10 *cm* per year, and can be considered to be a typical creeping landslide.

Three zones are distinguished in the landslide profiles based on the constituent clay minerals, *i.e.*, upper, slip and lower zones, respectively. The slip zone develops close to the boundary of the upper zone and the lower zone. Detailed examinations of microtexture indicate that the smectite rich landslide clays have undergone shearing deformation because the resulting texture is characterized by highly oriented parallel FF contacts. The landslide clays with highly oriented parallel FF contact texture have impermeable nature and the materials containing the clays are ready to start creep movement. Furthermore, cations such as Ca^{2+}, Mg^{2+} and Na^{+} derived from feldspar in the host rock are highly concentrated in the landslide clays, causing the increase of smectite content and at the same time promoting the replacement of Ca^{2+} and Mg^{2+} by Na^{+}. This reaction promotes the formation of Na-smectite or (Na, Ca)-smectite characterized by high expandability. This process further causes the decrease of soil strengths and the formation of characteristic microtexture, *i.e.*, lubrication plane. When the lubricating plane develops to a certain extent, the creeping landslide takes place.

The displacement rate of the creeping landslide mechanically depends mostly on the pore water pressure (groundwater level) in the landslide profiles. High pore water pressure always corresponds to the large displacement rate. Taking into consideration of groundwater levels and the mineralogical characteristics, a rheological model is proposed. Applying obtained soil constants to the model, the possibility of prediction of the creeping landslide is discussed, especially on the deformation process.

CONTENTS

I. Introduction

Landslide is one of the most destructive geological processes affecting human life and is a particularly troublesome natural hazard in Japan. The loss of human life, land and property due to landslide is a major social problem. The landslides occurring in Japan have been classified, generally in terms of geological factor, into three types, namely, Tertiary formation type, sheared zone type and hot spring type (Koide, 1955; 1962; 1963). The main cause of landslide, on the other hand, is divided into the internal factor and the inducing factor (Terzaghi, 1950; Veder, 1981). The former factor is geological and geomorphological features, and the latter rainfall, snow, groundwater, earthquake and so on (Aoki, 1986; Tamada *et al.*, 1986; Tamada and Fukuda, 1989). The occurrence of a landslide is a result of the combination actions of the internal and inducing factors (Veder, 1981; Zaruba and Mencl, 1982).

Tertiary formation type exceeds more than 67% of the all landslides occurring in Japan and, has occurred mostly in populated areas (Watari *et al.*, 1983). The occurrence mechanism of Tertiary formation landslides, especially with respect to mass movement, has been the intensive research subject (*e.g.*, Nishida and Tsushimoto, 1973; Yamanoi *et al.*, 1974; Shuzui, 1984; Shuzui and Nakamura, 1986; Shirahata *et al.*, 1987; Aramaki, 1987). From the geological standpoint, several intensive studies have been also published (Fujimoto, 1967; Takatani, 1972; Shuzui, 1984; 1986). Nishida and Tsushimoto (1973) reported that, in some landslide areas, smectite is a main constituent mineral among the landslide clays. Recently, Takeuchi and Takaya (1980) and Tamada (1984; 1986) pointed out that smectite content tends to increase toward a slip surface (or zone). These investigations indicate that landslides are controlled by geological characteristics, especially by clay minerals. However, detailed mineralogical characteristics of clay minerals in landslide area have not been sufficiently investigated up to the present.

Significance of micromorphological observation is recently pointed out in understanding of geotechnical properties of clay soils (Bennett *et al.*, 1981; Yamada, 1989). Especially, clay texture characteristics have a great influence on the shearing mechanism and deformation (Skempton, 1985). However, no systematic studies dealing with the microtexture characteristics of natural landslide clays have been made.

Furthermore, the study of forecast or prediction of landslide is advancing recently according to the recent progress of the geological and mineralogical science as well as those of technology. Studies on the prediction of deformation related to landslide are of particular significance not only in understanding of the deformation behavior but also in evaluation of long-term slope stability.

In this study, one landslide area located at Monden Town in the southwestern part of Okayama Prefecture, southwest Japan was selected for clarifying mechanism of Tertiary sediments landslide. The area has the following merits: (1) Large scale landslides have recently occurred in the area, and are still active at present; (2) The landslides are characterized by large displacements; and (3) The slip surfaces or slip zones are recognizable at depths less than 10 meters. The mineralogical and chemical characteristics of landslide materials were investigated. Based on the detailed study of clay minerals, such as smectite content together with its cation exchange properties in relation to landslide profiles and texture characteristics of landslide materials, the mechanism of landslide will be discussed. A rheological model was also developed for the purpose of prediction of landslide.

Acknowledgements

The author would like to express his sincerest gratitude and appreciation to Prof. Setsuo Takeno for his supervision, guidance and helping which aided the progress and completion of this work. He also wishes to express his deep gratitude and appreciation to Assoc. Prof. Ryuji Kitagawa of the Department of Earth and Planetary Systems Science for his valuable advice, encouragement, discussion and guidance. Particular thanks are due to Dr. Akira Yoshiasa of the same department for his helpful discussion and guidance.

The author is also indebted to Prof. Ikuo Hara, Yuji Okimura, Satoru Honda, Yuji Sano of the Hiroshima University, to Prof. Shigeru Iizumi of the Shimane University and to Prof. kazue Tazaki of the Kanazawa University for their guidance and advice. He is also grateful to Dr. Takao Yano of the Hiroshima University for his guidance and help.

The work is collaborated in part by Soil Division of Fukken Co. Ltd., Hiroshima. The author is greatly indebted to the chief, Katsumi Nakamori for his suggestion and comments.

The author wishes also to thank Hiroshima University and the Japanese Ministry of Education for providing the opportunity and scholarship to carry out this study at Hiroshima University.

II. Outline of geology

The investigated Monden landslide area is located in Monden Town, Ihara City, southwestern Okayama Prefecture, and situated in the southwestern part of the Kasaoka-Ihara-Tsuyama landslide zone with NE-SW trend (Landslide of Japan, 1973). As shown in Fig. 1, the coincidence between distributions of the Tertiary sediments and occurrence of landslides indicates that almost all landslides in Hiroshima-Okayama Prefectures occur in the Tertiary sediments. The Monden area is geomorphologically characterized by numerous small relief mountains of about 150 m above sea level. Low relief erosion surfaces are present at several horizons in the area. Landslides concentrate in a depressional area surrounded by hills at an altitude of 80 to 150 m, and occur mainly on a gentle slope at that of 60 to 80 m descending smoothly to an alluvial lowland of about 40 m altitude (Fig. 2). The hill top forms two low relief erosion surfaces at different levels. One spreads in the eastern part at an altitude of 120 to 160 m covered by gravel bed, and the other develops in the western part of the landslide area at an altitude of 80 to 120 m in the pre-Neogene basement rocks (Figs.

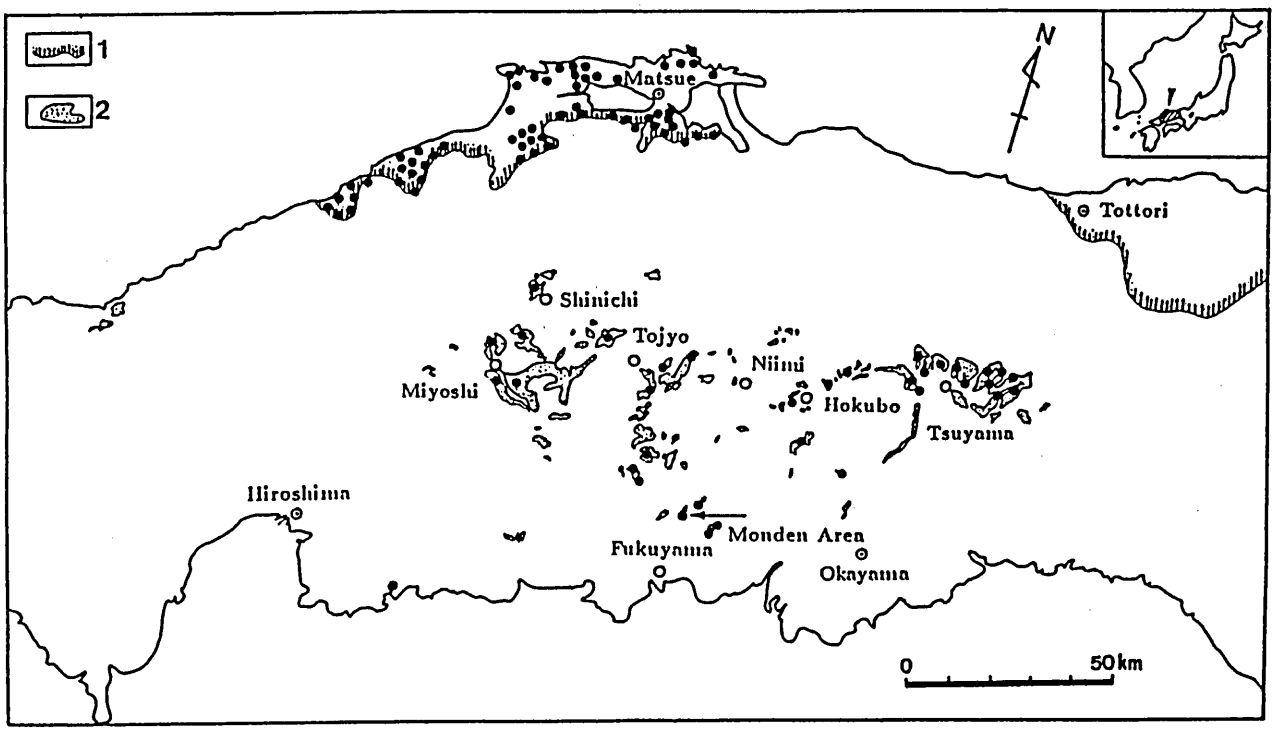

Fig. 1. Index map showing distribution of Tertiary sedimentary rocks (partly modified from Tai, 1975) and landslides in Chugoku district, Southwest Japan (data from Landslide of Japan, 1973).
1: Southern boundary of Tertiary green-tuff sediments, 2: Non-green tuff sediment, black circle: landslide area, open circle: location of Town.

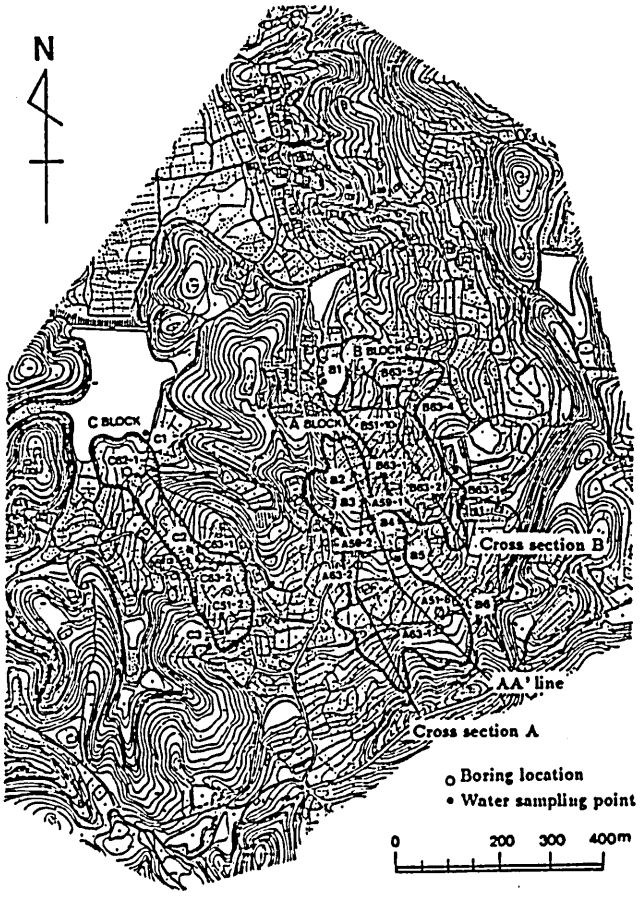

Fig. 2. Map showing distribution of sliding block and sampling location in Monden area.

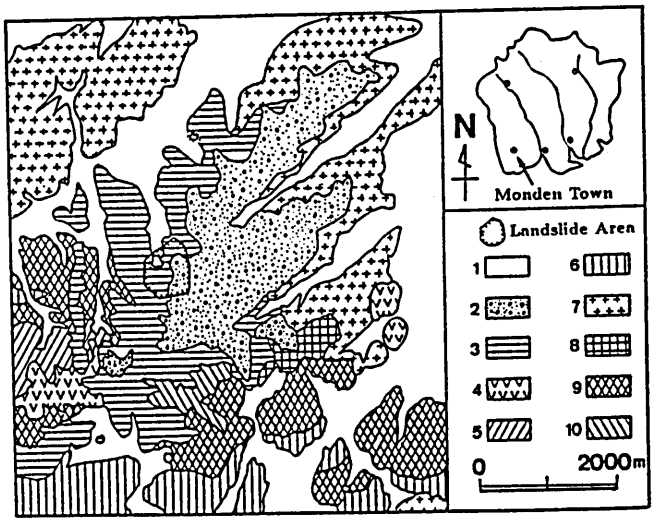

Fig. 3. Geological map of Monden area (partly modified from Mitsuno, 1985).
1: Alluvium, 2: Mountain gravels, 3: Nyokan formation, 4: Rhyolitic rock, 5: Acidic volcanic rock, 6: Gabbroic rock, 7: Granitic rock, 8: Basic tuff, 9: Slate, 10: Basic volcanic rock.

2 and 3). These hill top surfaces extend and gently dip toward the west-northwest.

In the Monden area, Paleozoic sediments, Cretaceous acidic volcanics and granitoids, Neogene sediments and Quaternary sediments are developed. The basement rocks of the area are composed of Paleozoic slate and basic rocks, Mesozoic rhyolitic and dacitic pyroclastics and granitic rocks (Tai, 1962; Mitsuno, 1985). The basement rocks distributed in the western part of the landslide area form a lowland and expose over the low relief erosion surface. The granitic rocks are distributed in the eastern part of the area (Fig. 3).

The acidic volcanics has a resistant nature accompanying with relatively thin weathering crust of about 3 *m* thick. The granitic rocks, on the other hand, are remarkably weathered with saprolite layer of about 15 *m* thick in an extensive area.

The Neogene sediments, designated as Nyokan formation (Tai, 1962; Mitsuno, 1985), uncomfortably overlie the basement rocks, and gently dip downslope with about 10 degrees and the direction is the same to that of landslide slope (Public Works Office, Okayama Prefecture, 1990). The Nyokan formation of lacustine origin is composed of alternation of tuffaceous sandstone and mudstone. The sandstone is from 4 to 6 meters in thickness and is fine to coarse grained massive sediments with brownish gray to yellowish brown color. The mudstone called the Kasaoka clay (Tai, 1962) exceeds 10 meters in thickness in the landslide area and is homogeneous, gray to blackish gray in color. The landslides in the area tend to take place in the mudstone area.

The Neogene sediments are highly weathered and softened extensively resulting clay soil. In the Neogene sedimentary rocks, fissure and/or cracks parallel to bedding plane are well developed especially in mudstone, probably due to swelling and shrinkage of rock volume in response to seasonal fluctuation of the groundwater levels.

The Quarternary gravel layer, called Mountain gravels (Tai, 1962; Mitsuno, 1985), uncomfortably overlies the Neogene sediments and crops out in the eastern part of the area (Fig. 3). The Mountain gravels in the area ranges in thickness from 5 to 30 meters. It mainly consists of pebble gravels of 2 to 40 *cm* in grain size and contains an intercalated coarse sandstone beds of 10 to 30 *cm* thickness. The generalized stratigraphy of the landslide area is shown in Fig. 4 which is partly based on the boring core observation.

Quaterary	Alluvium	clay, sand, gravel	5～20 m
	Mountain Gravels	gravel, sand, clay	5～30 m
Neogene	Nyokan Formation	sandstone	4～6 m
		mudstone	10 m+
Mosozoic to Paleozoic	Basement Rocks	granitic rock, dacitic rock, rhyolitic rock, basic rock, slate.	

Fig. 4. Generalized stratigraphy of the landslide area.

Based on field and boring core observations, the Neogene and Quaterary sediments in the southeastern parts of the area dip 10 degrees to south, whereas those in the southwestern part dip 10 degrees to north. Therefore, a basinal structure of syncline is recognized in the area trending northeast-southwest direction (Public Works Office, Okayama Prefecture, 1990).

III. Landslide description

The geomorphological and fracturing features show that the Monden landslide area can be subdivided into three sliding blocks (Fig. 2). These sliding blocks have an altitudinal difference of about 50 *m* and slope lengths of 300 to 500 *m*, and all of the three blocks gently dip about 10 degrees to north (Fig. 2). Inclinometer measurement shows that landsliding in the area occurs within mudstone layer, and the slip zones at about 5.0 to 6.5 *m* depths dip parallel to geographical slope and adjoin the natural pond at the foot of the slope (data from Public Works Office, Okayama Prefecture, 1990) (Figs. 2 and 5).

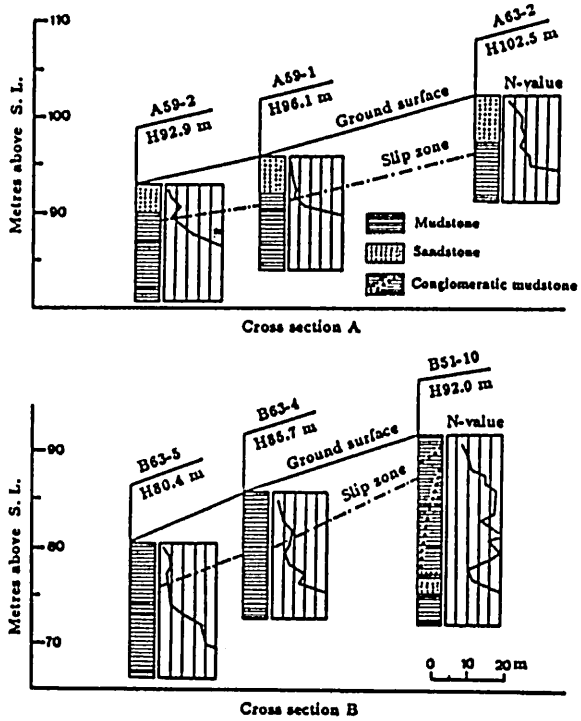

Fig. 5. Cross-section of the landslide area showing slip zone almost parallel to ground surface.

The first signs of landslide were observed in August 1975 following a heavy rainfall in July 1975 (Public Works Office, Okayama Prefecture, 1984; 1990). After that, the landslides became gradually dormant to creep movement but only at instrumentally detectable rate less than 10 *mm* per year. Since September 1984, the landslides were activated again, subsequent to a continuous rainfall during June to July 1984. The total downhill displacement amounted to about 100 *mm* during September 1984 to January 1990.

The presence of the Monden landslides can be recognized chiefly from geomorphological evidence of a deflated

gentle slope, scarps and tensional crack around the head of the landslides and the squeezed toe. Fig. 6 schematically illustrates the topographic details and the relevant terms identified in the landslide area. Cracks are generally formed by defferential shearing between the moving mass and the inactive mass in landslide area (George *et al.*, 1978). Therefore, the main scarps observed in the area are considered to be as the head limit of the slide block. Another clear signs of active landsliding are recognized by intense cracking and fissuring of several buildings and constructions.

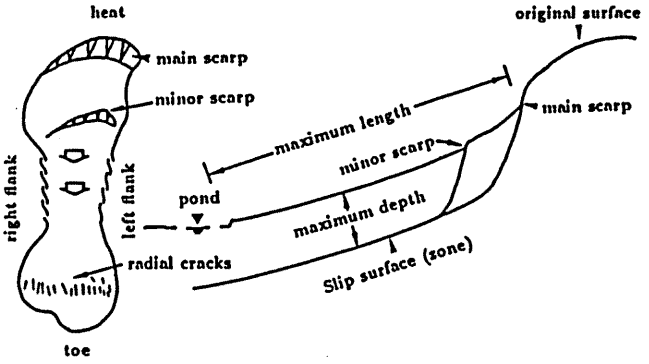

Fig. 6. Topographic details and relevant terms identified in the landslide area.

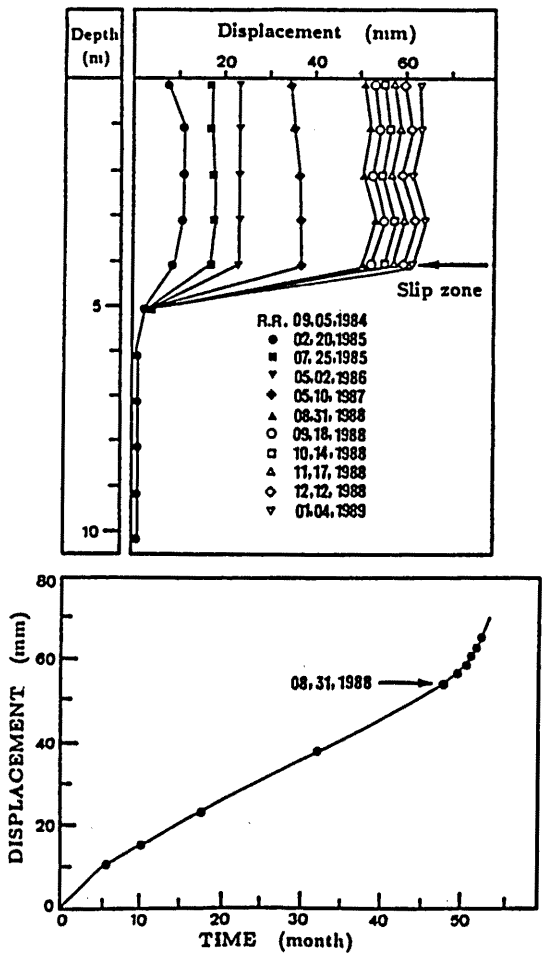

Fig. 7. Displacement and depth curve of the Monden landslide.
The data were obtained in hole A59-2.

To obtain the underground information of the landslide area, 15 boreholes were drilled by Fukken Co. Ltd., Hiroshima as shown in Fig. 2 (open circle). Fig. 7 shows the nature and extent of landsliding observed at the inclinometer hole *A*59-2 in the sliding block *A* (Fig. 2) during September 1984 to January 1990 (data from Public Works Office, Okayama Prefecture, 1990). As is evident in this figure, normal slow movement of the landslides is accelerated after accidental large displacements in July 1988 (arrow) due to heavy rainfall, and the figure also indicates that the landslides in the area have slow creep characteristics at the rate of 2 to 10 mm/yr.

IV. Sampling and methods

A. Sample sites and sample selection

Fig. 5 shows two cross sections constructed from the boring cores observation. As shown in Fig. 5, the cross sections *A* and *B* (illustrated in Fig. 3) represent the geological characteristics of the landslide area. Two detailed examples of the profile are given in Fig. 8, one is obtained at the borehole *A*63 – 2 in the cross section *A*, and the other at the borehole *B*63 – 4 in the cross section *B*. As is evident in Fig. 8, the former is composed of sandstone and mudstone, and the latter consists of only mudstone.

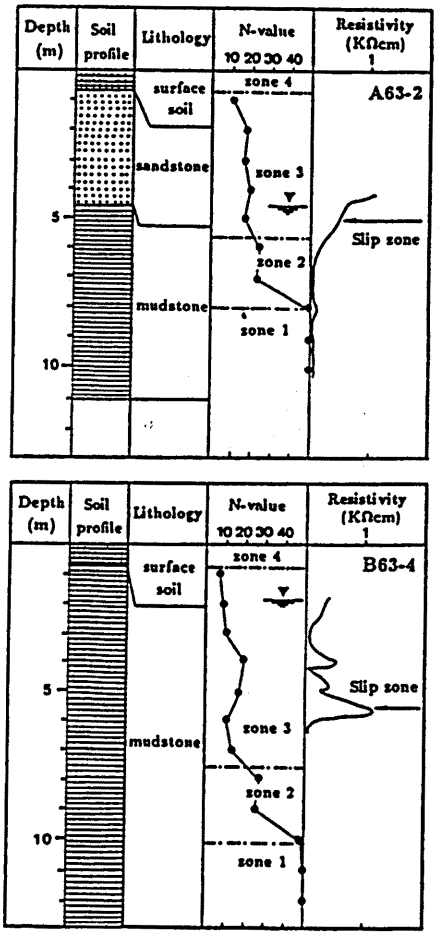

Fig. 8. Geological characteristics and the in situ test data of the studied profiles of A63-2 and B63-4.

In the landslide profile *A*63 – 2, the sandstone of more

than 4.5 meters thickness overlies the mudstone, and the sandstone is brownish gray to brown fine-grained sediments with silt and clay fractions; the mudstone is homogeneous and gray in color. The boundary between the sandstone and the mudstone corresponds to the transition zone between brown oxidized sediments and gray sediments. Small amount of pyrite crystals of about 1.5 *cm* in size were observed under a binocular microscope in both sandstone and mudstone. On the other hand, the landslide profile $B63-4$ is composed only of the mudstone, which is homogeneous, white gray to light green fine-grained sediments and contains small amount of silt and sand fractions.

In Fig. 8, in situ test data of groundwater resistivity and N-value measured by Standard Penetration Test (SPT) are also indicated. The variation of N-value in sedimentary rocks corresponds generally to the degree of weathering (Matsukura and Mizuno, 1986; Miura, 1987). Therefore, N-value can be used as the degree of weathering (Matsukura and Mizuno, 1986). In the present research, the profiles of $A63-2$ and $B63-4$ are both divided into four zones (Fig. 8) on the basis of the N-value: Zone 1 (N larger than 50) showing no discoloration caused by oxidation and difficult to break by fingers; Zone 2 (N ranging from 20 to 50) retaining original rock texture and can be considered weakly weathered sediments; Zone 3 (N less than 20) which is easily deformed and smeared by fingers; and Zone 4 (surface soil) which is of black gray to black clay soil containing a small amount of gravel-size clasts and plant remains. These zones correspond roughly to fresh or weakly weathered rocks, moderately weathered rocks, remarkably weathered rocks and surface soils, respectively. The slip zone of the landslides in the area is found mainly in Zone 3.

The analyzed samples were taken from the landslide profiles of $A63-2$ and $B63-4$ (Fig. 8) at interval of 50 *cm* from the surface to the maximum of 12.5 *m* depth.

B. Analytical methods

Since the mineralogical composition and physicochemical properties of clay fraction (less than 2 μm) are the most important factor governing the shearing (Lupini *et al.*, 1981; Skempton, 1985), analyses were carried out on both the bulk and clay fraction samples. The clay fraction (less than 2 μm) was separated after dis-aggration in distilled water using ultrasonic wave.

X-ray diffraction Mineral constituents of the bulk and the clay fraction samples were determined by an X-ray diffractometer using Ni-filtered $CuK\alpha$ radiation. The constituent minerals of the bulk samples are composed mainly of feldspar, quartz and clay minerals of 15 $\AA$, 10 $\AA$ and 7.2 $\AA$ basal spacings. To identify clay minerals, the following three analyses were made: (1) untreated air-dried conditions; (2) treatment with ethylene glycol; and (3) heating at $300°C$ and $600°C$ for one hour. Semiquantitative estimates of the amount of the respective constituent minerals were made by measuring peak height of the diffraction of the air-dried samples as described by Tanaka *et al.* (1991).

Suspension pH Suspension pH values are considered to represent the H ion activities around mineral grains and can be thus used as an indicator of weathering environments. Suspension pH measurement was made by mixing the 30 *mg* of powdered sample with 50 *ml* distilled water according to the method described by Chigira (1987; 1988; 1990), and the value was measured using a Digita HM-20B pH meter.

Exchangeable cation Landslide clays, especially in Tertiary sedimentary rocks, includes various clay minerals and most of the clay minerals are usually changed their mineralogical characteristics by rain and groundwater. In addition, cations in clay minerals are easily exchangeable (Matsuo *et al.*, 1979). Cation exchange causes the weakness of soil strengths (Matsuo, 1957; Moore, 1991). The exchangeable cation analysis was carried out on the clay fractions displacing the exchangeable cations by successive washing with 1 N $SrCl_2$ solution (Wada, 1981; Sridharan *et al.*, 1987). Amount of the displaced calcium, magnesium, sodium and potassium ions were determined using a Shimadzu AA-646 atomic absorption/flame emission spectrophotometer.

Cation exchange capacity (CEC) is the sum of the exchangeable cations. Ion exchange reaction affects extensively the physicochemical and mechanical properties of soil, is considered to be one of the main causes of landslide (Matsuo and Tomita, 1970a, 1970b). Cation exchange capacities were determined according to the methods described by Wada (1981) and Sridharan *et al.* (1987). That is, about 100 *mg* of clay fractions was saturated with 1 N $SrCl_2$ solution and washed successive with distilled water. The saturated sample was then prepared for atomic absorption spectroscopy analysis. Contents of Sr in the saturated sample were determined by using a Shimadzu AA-646 atomic absorption/flame emission spectrophotometer. CECs were calculated on the basis of Sr $meq/100mg$ of the respective sample.

Chemical analysis Detailed chemical composition of soils is indispensable to determine the constituent clay minerals, leaching condition and the degree of weathering. The contents of $Ti, Al, Fe, Mn, Mg, Ca, Na$, and K were determined using a Shimadzu AA-646 atomic absorption/flame emission spectrophotometer, and the obtained values were calculated and expressed in the form of oxide. The content of Si was not determined because of technical difficulties of sample preparation for atomic-absorption method.

Groundwater chemical analysis Occurrence of landslides relates intimately to ground and/or surface water. The quality of ground and surface water in landslide area offers the information of underground environments such as distribution of cations and weathering reaction (Isagai *et al.*, 1990). The groundwater and surface water were collected within the landslide area in washed polyethylene bottles (Fig. 2). The groundwater at $a4$ and $c2$ was taken from drain borehole in which the slip zone is present. The surface water was taken from natural ponds near the toe of landslide blocks (samples $a1, a2$, and $c1$) and in the neighboring area of the sliding heads (samples $a3, a5, a6$ and $c3$). Chemical composition was determined for anions with a Tosho Model HLC-803D anion exchange chromatography, and for cations with a Shimadzu AA-646 atomic absorption/flame emission spectrophotome-

ter, respectively.

SEM observation Because of the high vacuum conditions in scanning electron microscope, all samples must be dehydrated before viewing. Dehydration may deform the microctexture since the high surface tension of water yields strong stresses on the individual particles and causes reorientation. Several methods have been developed for SEM observation such as critical point drying (CPD), freeze drying (FD) and air drying (AD) (Reynolds and Gorsline, 1991). AD method, slow dehydration at atmospheric condition, has been widely used for observation of aggregation texture (Baracos, 1976). In this study, specimens for SEM observation were dehydrated by AD method. After dehydration, fresh surfaces both parallel and normal to the slip zone were prepared for SEM observation. Air-dried specimens were manually trimmed to about 1.5 by 1.5 *cm* in cross section, and 3 to 4 *cm* in length, and then carefully bent and pulled, to initiate fracture. Specimens with clear cleavage were cleaved to provide fresh fracture surface by prying with a knife along cleavage surfaces. The prepared specimens were cemented on SEM mounting stubs so as to be the fresh fracture surfaces upward, and observed using scanning electron microscope.

Moreover, in order to examine the effects of shearing processes on particle arrangements, the landslide clay samples taken from borehole $A59-2$ (Fig. 5) at depths of 50 to 70 *cm* were sheared by direct simple shear apparatus and then prepared for SEM observation both parallel and vertical to the shearing zone.

Optical microscope observation Thin sections both parallel and perpendicular to the slip zone were prepared for optical microscope observation. The landslide materials, dominated by expansive clay minerals, readily expand when subjected to hydration. Therefore, specimens were first indurated with cyunobond before making thin section, and then ground without water to prevent softening.

Particle orientation Direct and indirect techniques for the evaluation of particle arrangements are available such as polarizing microscopy, X-ray diffraction and electron microscopy (Yong, 1971; Yong and Warkentin, 1975). XRD analyses are particularly useful in quantifying the particle orientation (Yong, 1971). To use the XRD method for investigating preferred particle orientation of clay minerals, it is noted that the specimens tend to prefer the basal planes and the reflection intensity of the other planes decreases considerably. In this paper, orientation index, I_o, is introduced to evaluate the degree of preferred orientation, and defined as follows:

$$I_o = I_h/(I_h + I_v)$$

Where I_h and I_v are the peak intensities of clay minerals parallel and perpendicular to the slip zone of the respective samples, respectively.

Examination of the orientation index was performed using the intensity of X-ray diffraction. Thin sections both parallel and normal to the slip zone of the same sample were determined by X-ray diffractometer with $CuK\alpha$ radiation under the conditions of 30 KV and 10 mA. The orientation index I_o was calculated based on the above formulae, $I_h/(I_h + I_v)$, after examining the I_h and I_v.

Creep test To determine the relevant geotechnical parameters in constitutive equations, laboratory test simulating the in situ loading conditions as closely as possible was performed. The direct simple shear apparatus is an important tool for determining shear strength parameters in slope stability analysis, because the shearing process is analogous to plane strain problem such as creep deformation of slope (Nakamori and Yang, 1991; Yang *et al.*, 1993). However, the apparatus has a fundamental defect with which pore water pressure can not be controlled during shearing deformation (Saada and Townsend, 1981). Moreover, it is well recognized that landslide occurrence is almost associated with heavy rainfall (Aoki, 1986; Tamada and Fukuda, 1991). That is, the change of groundwater level is one of the main inducing factors for landslide occurrence. In the present research, direct simple shear apparatus was modified so as to control pore water pressure corresponding to the change of groundwater levels in landslide slope.

Fig. 9 schematically shows loading system with shearing cell and fluid pressure control (Yang *et al.*, 1993). The water pressure can be controlled by adjusting the air pressure (G_3), and the air pressure is maintained constant with help of G_3 during a test. The cylindrical soil sample, 25 *cm* high and 60 *cm* in diameter, is surrounded by a series of plastic rings and a rubber membrane so that the drainage condition could be controlled. The water pressure is applied directly to the top of sample. The resulting pore water pressure is measured by pore water gauge pressure (G_2) at the base. The horizontal shear displacement is measured by displacement gauge (G_1).

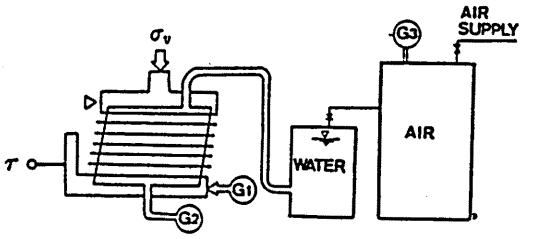

Fig. 9. Schematic description of direct simple shear apparatus.
σ_v: vertical stress, τ: shear stress, G_1: displacement gauge, G_2: pore water pressure gauge, G_3: air pressure gauge.

Since landslide clays are generally very thin, a large number of undisturbed samples for direct simple shear test are difficult to take from landslide clays. Therefore, three sets of direct simple shear tests were first performed on remoulded kaolin samples to determine the creep characteristics associated with the pore water pressure changes. The kaolin samples were first preconsolidated at vertical stresses of 100 kPa and 150 kPa, respectively, and then were prepared for creep tests. The test conditions are given in Table 1. In set 1, the vertical stress (σ_v) and the water pressure (u) were set to 100 kPa and 0 kPa with variable shearing stress (τ_h) of 3 to 20 kPa, respectively. In order to determine the effect of the pore water pressure on horizontal displacement, in set 2, the water pressure was set to 40 kPa with the same vertical and shearing stresses to those of set 1. Furthermore, in set 3, tests were carried out under the condition of in-

creasing water pressure and of the constant vertical and shearing stresses to determine the effect of the individual water pressure factor on the creep displacement.

Table 1. Test conditions of direct simple shear tests for remoulded kaolin sample.

TEST	σ_v (kPa)	τ_h (kPa)	u (kPa)
SET 1	100	3 - 20	00
SET 2	100	3 - 20	40
SET 3	150	30	20 - 80

To examine the relationship between the creep behavior and the pore water pressure changes, direct simple shear tests were also carried out on the undisturbed landslide clays collected from the investigated area. The clay samples were taken from borehole $A59-2$ at a depths of 50 to 70 cm (Fig. 2) in which the slip zone occurs. The average physical properties of the tested clays are as follows: natural water content W_n, 32.97%; plasticity index I_p, 27.31; specific gravity of soil particle ρ_s, 2.68 g/cm^3; wet density ρ_t, 1.78 g/cm^3. The applied stresses for direct simple shear tests were calculated using the following formulae:

$$\tau_h = \sigma_x = (h_c\rho_t + (H - h_c)\rho_{sat})\cos\theta\sin\theta$$
$$\sigma_v = \sigma_z = (h_c\rho_t + (H - h_c)\rho_{sat})\cos^2\theta$$

Where τ_h is the shearing stress, σ_v the vertical stress, H the depth of the slip zone, h_c the depth of the groundwater level, θ the gradient of the slip zone.

Here, H and θ are 60 cm and 10 degrees, respective, because the slip zone occurs at the average depth of 60 cm with slope of 10 degrees. The groundwater levels are 0, 10 and 35 cm during heavy rainfall, rainy season and dry season, respectively (Public Works Office, Okayama Prefecture, 1990), the h_c values is thus assumed to be 0, 10, and 35 cm, respectively, corresponding to the changes of the groundwater levels. Table 2 gives the applied stresses for direct simple shear tests.

Table 2. Applied stress of direct simple shear tests for Monden landslide clays.

TEST	σ_v (kPa)	τ_h (kPa)	u (kPa)
TEST 1	90	16	25
TEST 2	100	18	50
TEST 1	109	19	60

V. Experimental results

A. X-ray diffraction analysis

The representative X-ray diffraction (XRD) patterns of the bulk and the clay fraction samples collected from the two landslide profiles ($A63-2$ and $B63-4$) are illustrated in Figs. 10 and 11, respectively. As is seen in these figures, the constituent minerals of the landslide profiles are composed mainly of feldspar, quartz and clay minerals.

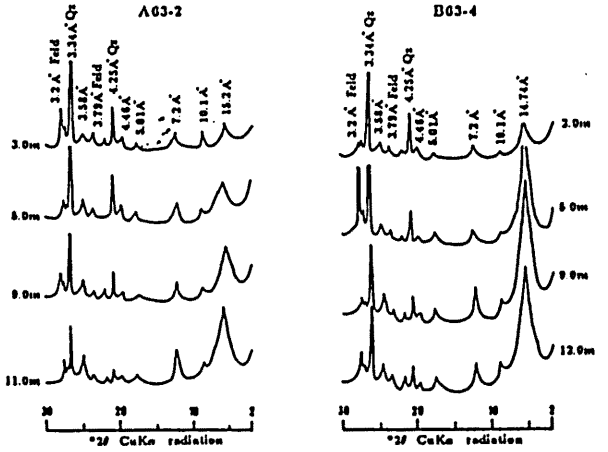

Fig. 10. Representative XRD patterns of the bulk samples from the landslide profiles of A63-2 and B63-4.

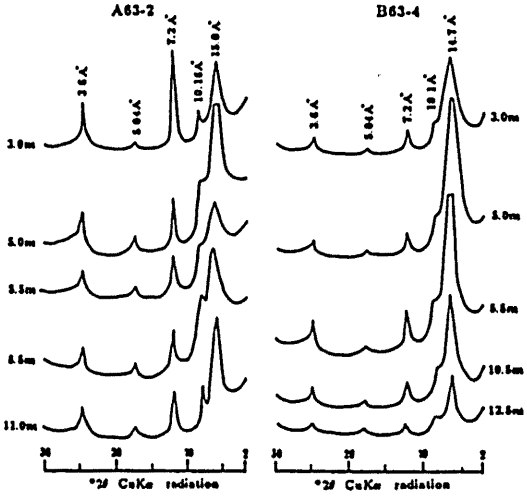

Fig. 11. Representative XRD patterns of the clay fraction samples from the landslide profiles of A63-2 and B63-4.

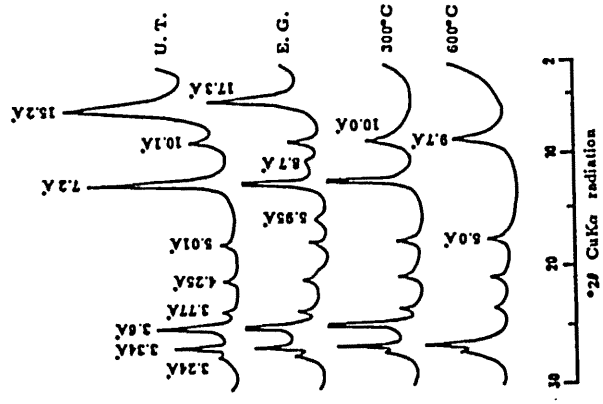

Fig. 12. XRD patterns for samples A2.0 (from landslide profile A63-2 at 2.0m deep) before and after various treatments.
U.T. : untreated, E.G. : ethylene glycol treatment.

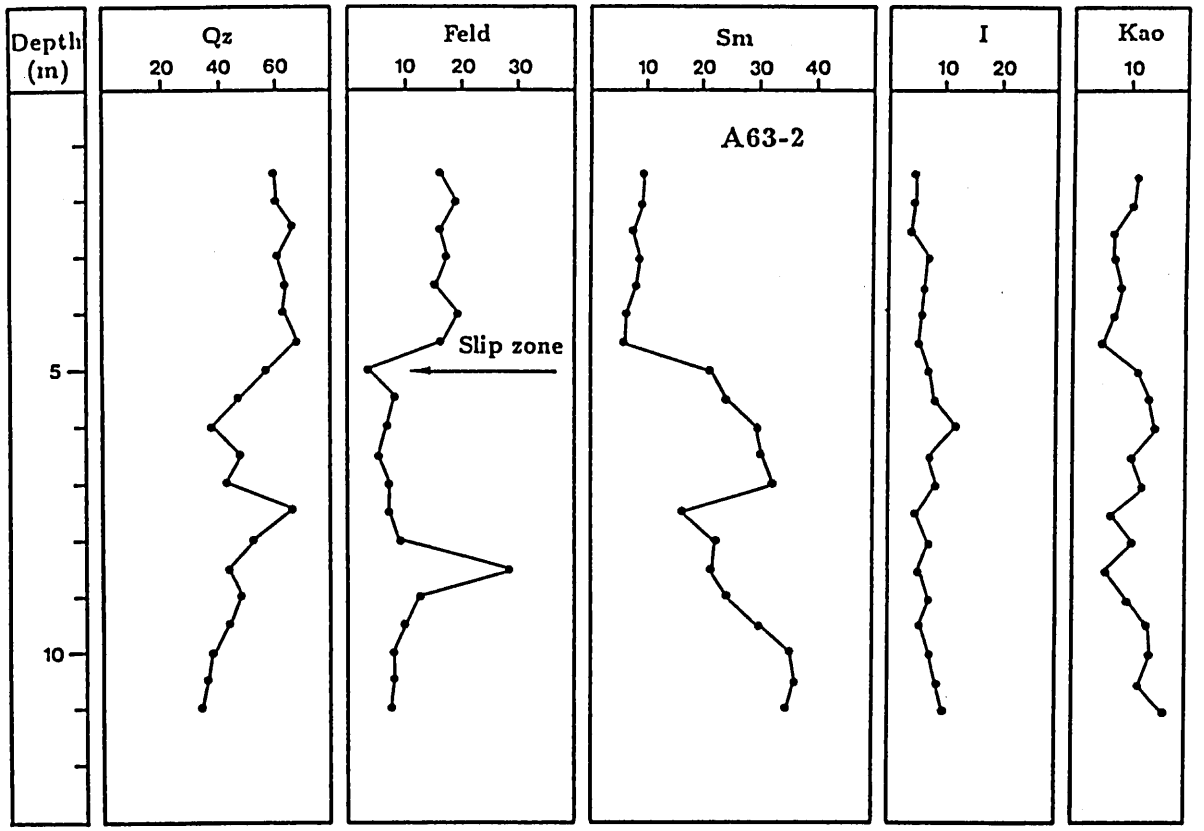

Fig. 13. Variation of the constituent minerals of the bulk samples from the landslide profile A63-2 as a function of depth.
Qz: quartz, Feld: feldspar, Sm: smectite, I: illite, Kao: kaolin minerals.

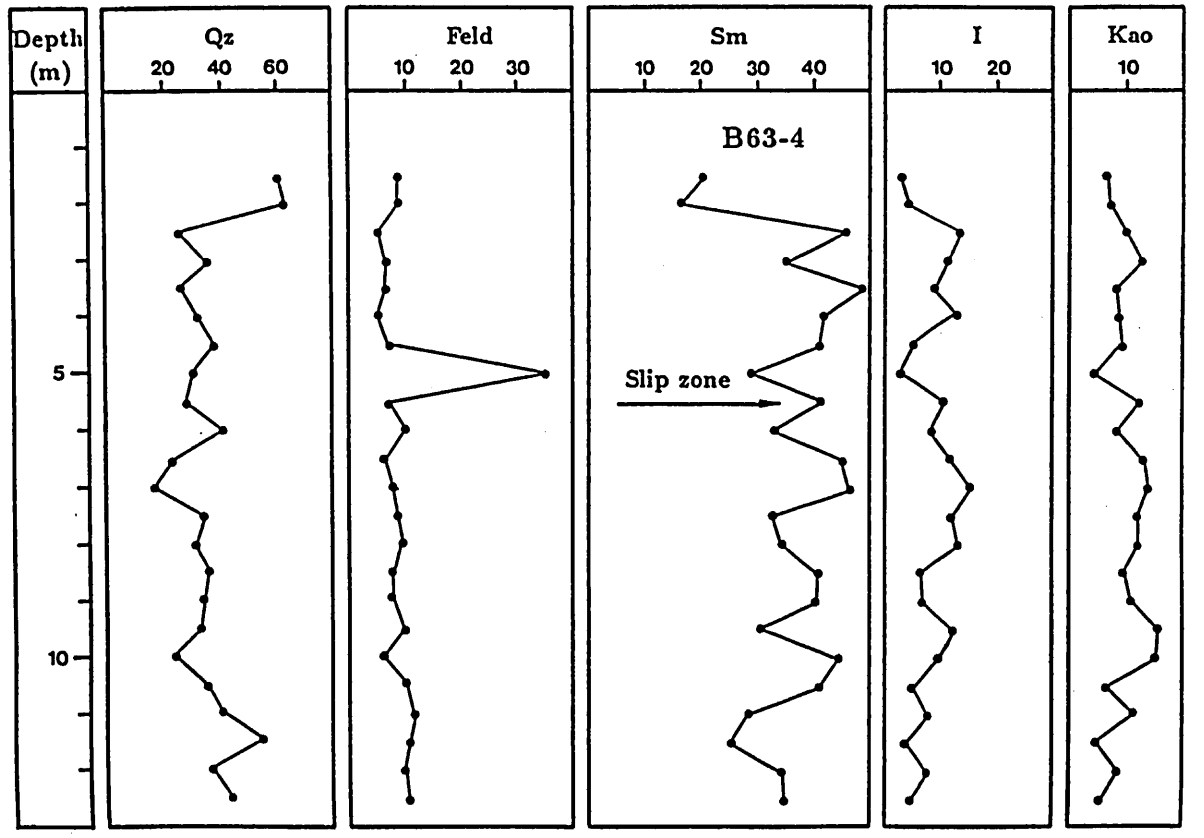

Fig. 14. Variation of the constituent minerals of the bulk samples from the landslide profile B63-4 as a function of depth.
Qz: quartz, Feld: feldspar, Sm: smectite, I: illite, Kao: kaolin minerals.

Fig. 12 shows the representative XRD patterns after various treatments for sample A2.0 collected from the profile $A63-2$ (2.0 m deep). The 15.2 $\AA$ basal spacing expands to 17.3 $\AA$ by ethylene glycol treatment, and almost completely contracts to 10.0 $\AA$ after heating at 300°C for one hour and to 9.7 $\AA$ at 600°C for one hour, respectively. The results indicate that the 15.2 $\AA$ basal spacing is smectite.

The 10.1 $\AA$ basal reflection remains unchanged by ethylene glycol treatment. By heating at 600°C for one hour, the intensity of the 10.1 $\AA$ reflection increases without changing the spacing. Therefore, the 10.1 $\AA$ mineral is considered to be mica clay mineral or illite. The 7.2 $\AA$ and 3.6 $\AA$ reflections remain stable at least up to the temperature of 300°C and disappear at 600°C, and are thus identified as kaolin minerals.

Variation of the constituent minerals in the two landslide profiles were semiquantitatively determined by XRD analysis for the bulk and the clay fraction samples, and the obtained results are plotted on Figs. 13, 14 and 15, respectively. The XRD semiquantitative analysis using the reflection intensities normalized to 100% shows relative abundance of the constituent minerals.

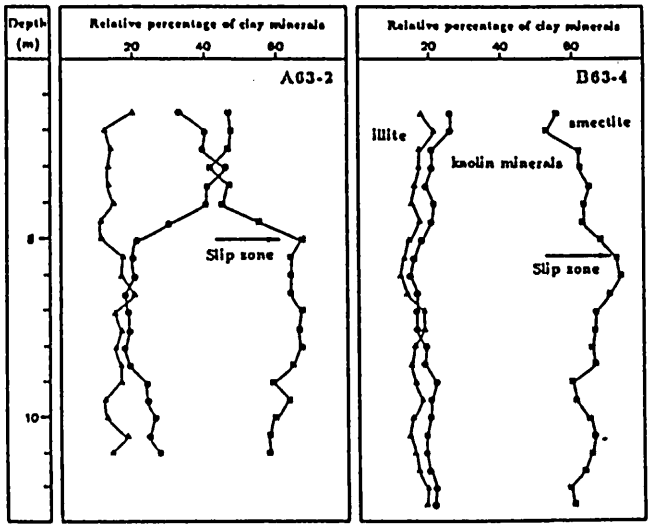

Fig. 15. Variation in relative abundance of smectite, illite and kaolin minerals with depth in the clay fraction samples.

As shown in Fig. 13, in the landslide profile $A63-2$, quartz content decreases with increasing depth whereas feldspar content decreases with depth, except for the sample of 8.5 m depth. Smectite content, on the other hand, increases from about 10% to 30% with increasing depth. Contents of illite and kaolin minerals are about 5% and 10%, respectively, showing little variation with depth. In the landslide profile $B63-4$, no clear tendency with depth is recognized (Fig. 14). Quartz and feldspar contents are constant with the exception of sharp increase of feldspar in 5.0 m deep. Smectite, illite and kaolin minerals contents are about 40%, 10% and 10%, respectively, showing no distinct change with depth.

Finer particles such as clay fractions (less than 2 μm) are generally considered to be the product of weathering (Calvert *et al.*, 1980). Therefore, the variation of relative amount of clay minerals in the clay fraction samples will reflect the mineralogical transformations during the processes of weathering. Fig. 15 presents the variation of relative abundance of smectite, illite and kaolin minerals in the clay fraction samples in the two landslide profiles. The clay fraction samples are composed mainly of smectite, illite and kaolin minerals with small amount of quartz (less than 5%). As is evident in Fig. 15, variation of the constituent clay minerals with depth in the two landslide profiles are quite similar with each other. Smectite content increases rapidly with depth until the slip zone and, from that point it decreases slightly. Kaolin minerals show an inverse variation to smectite with depth. The two clay minerals are contained in inverse proportions in the clay fraction samples for the two landslide profiles.

Fig. 16 illustrates the variation tendency of expandability of smectite with increasing depth in the two landslide profiles. The basal spacings of smectite at atmospheric condition (open symbol) differ with depth in the two profiles, suggesting that the interlayer cations change with increasing depth (Iwasaki and Watanabe, 1988). Furthermore, spacings of smectite at 100% relative humidity (black symbol) also vary with depth, showing clearly that the amount and types of interlayer exchangeable cations of smectite differ with depth (Odom, 1984; Moore and Hower, 1986; Iwasaki and Watanabe, 1988). Basal spacings of smectite collected from the slip zone (Fig. 16, arrow) change from 14.7 $\AA$ at atmospheric condition to 18.8 $\AA$ at 100% relative humidity. The fact suggests that smectite in the slip zone has predominant interlayer Na ions (Moore and Hower, 1986; Watanabe and Sato, 1988).

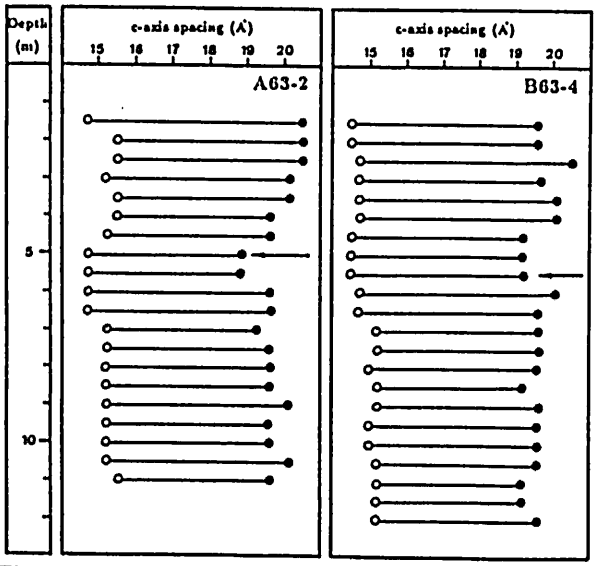

Fig. 16. Swelling and hydration properties of smectite.
Open circle: at atmospheric condition, black circle: at 100% relative humidity.

B. Exchangeable cation analysis

As was described in the previous (Figs. 13, 14 and 15), the landslide materials contain predominant smectite and the mineral has a high activity and easily exchanges contained cations in the presence of groundwater. The exchangeable cation contents of the clay fractions in the

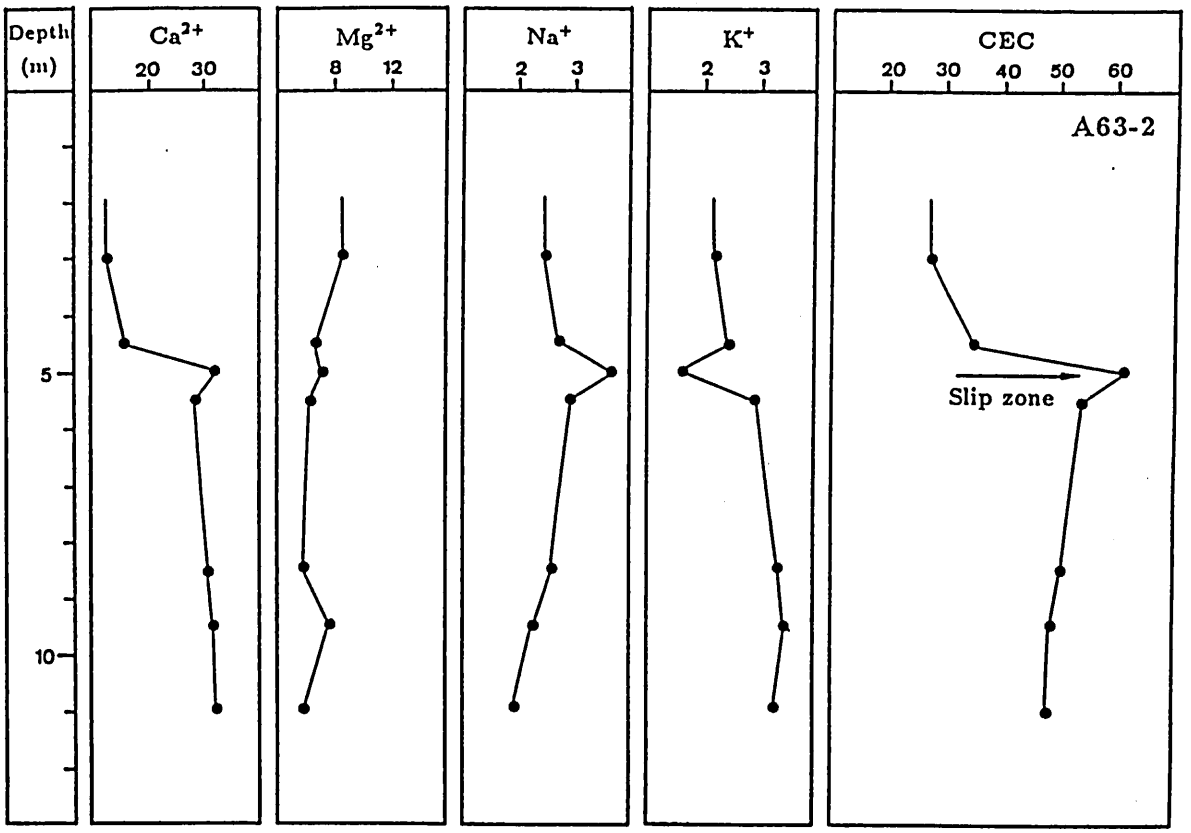

Fig. 17. Variation of exchangeable cation contents (meq/100g) and CECs (meq/100g) with depth for the clay fraction samples from the landslide profile A63-2.

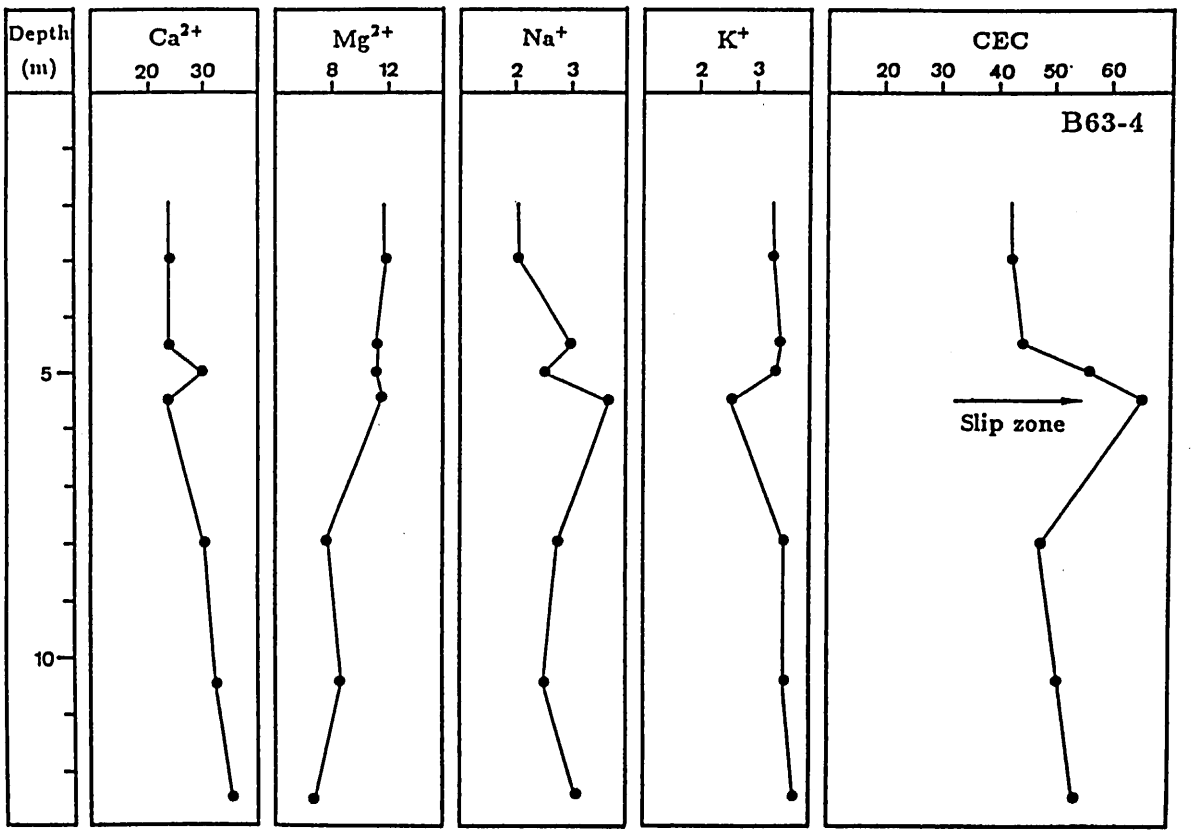

Fig. 18. Variation of exchangeable cation contents (meq/100g) and CECs (meq/100g) with depth for the clay fraction samples from the landslide profile B63-4.

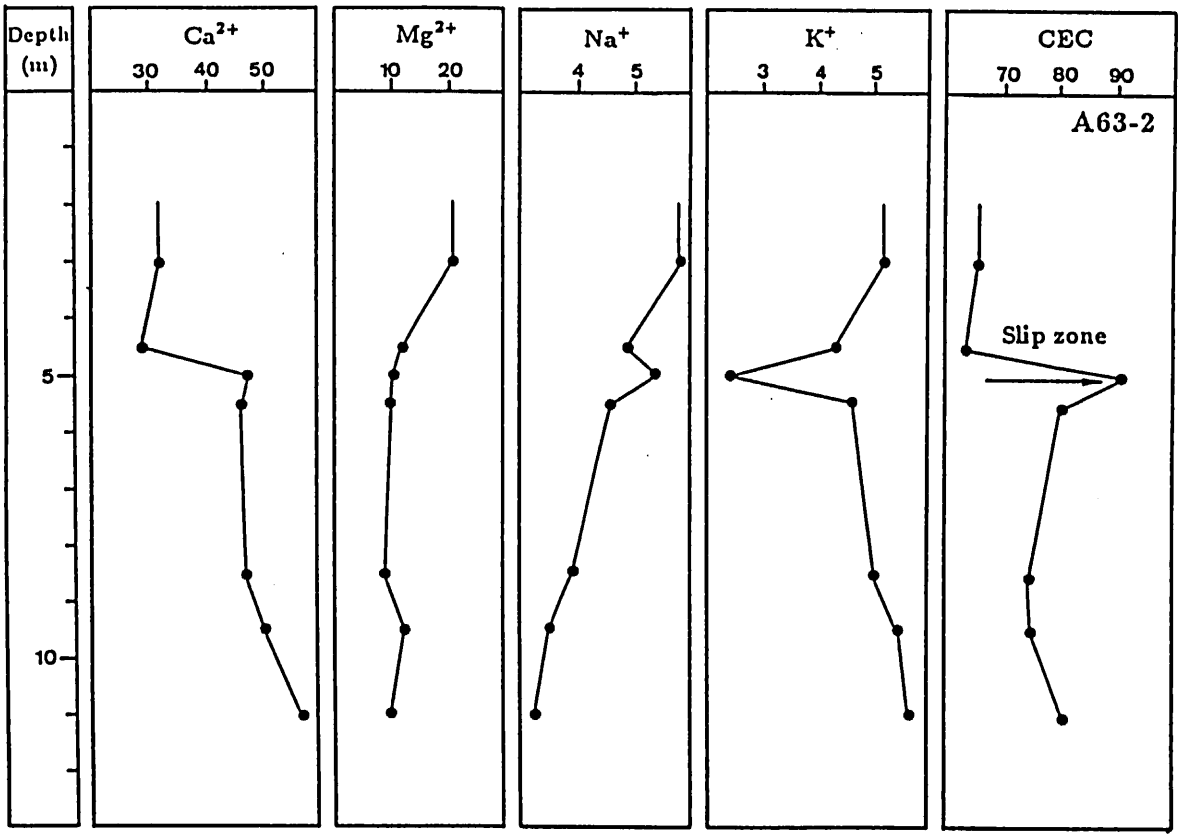

Fig. 19. Variation of exchangeable cation contents (meq/100g) and CECs (meq/100g) of smectite in the landslide profile A63-2.

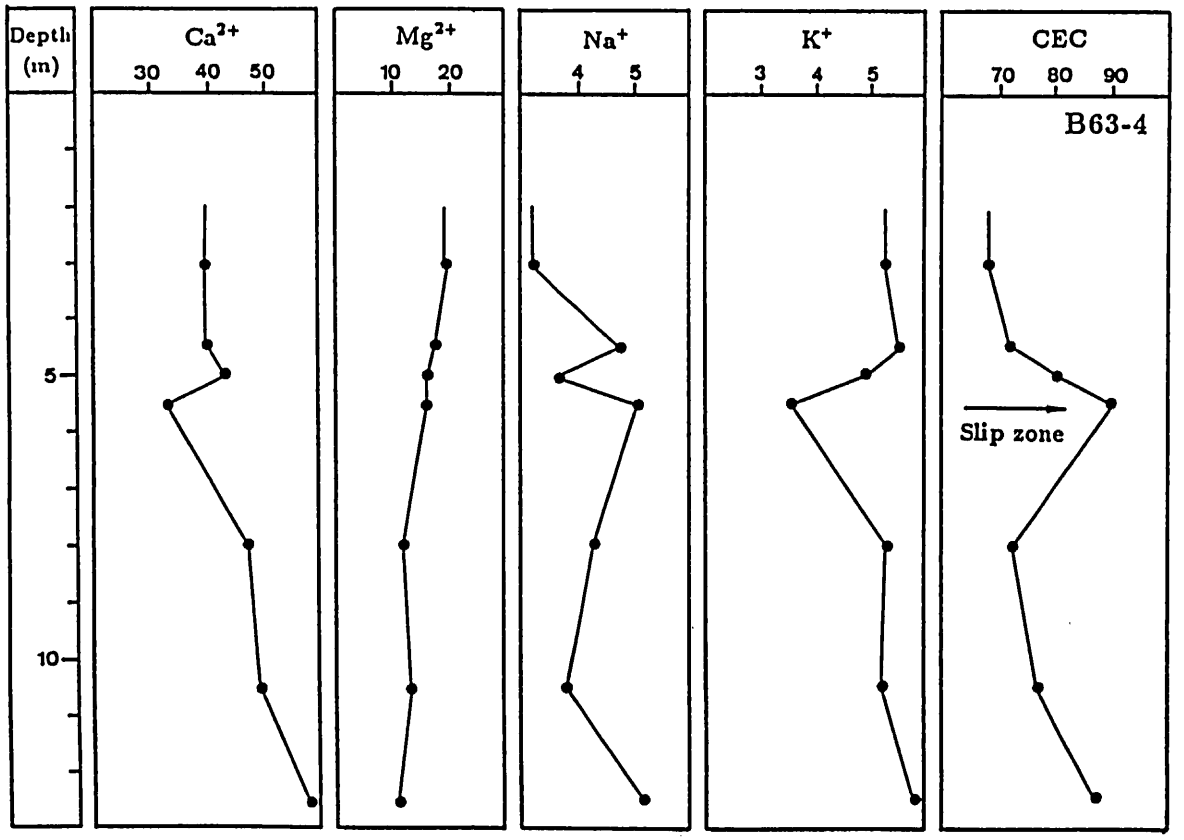

Fig. 20. Variation of exchangeable cation contents (meq/100g) and CECs (meq/100g) of smectite in the landslide profile B63-4.

landslide profiles $A63-2$ and $B63-4$ are presented in Table 3 and illustrated as a function of depth in Figs. 17 and 18, respectively. The exchangeable cation contents and CECs change suddenly near the slip zone in the both landslide profiles (Fig. 17 and 18). High concentration of exchangeable Ca^{2+} ion (Table 3) can be ascribed to the dominant cation Ca in the host rock of the landslide materials. Moreover, to be noted is high Na^{+} concentration and low K^{+} concentration near the slip zone.

Table 3. Exchangeable cation contents of the clay fraction samples.

Depth	Ca^{2+}	Mg^{2+}	Na^{+}	K^{+}	CEC
m	meq/100g	meq/100g	meq/100g	meq/100g	meq/100g
landslide profile A63-2					
3.00	13.19	8.69	2.46	2.17	27.15
4.50	16.00	6.61	2.72	2.38	35.25
5.00	32.44	7.15	3.66	1.64	61.52
5.50	29.23	6.42	2.90	2.90	54.21
8.50	31.16	6.01	2.59	3.27	50.13
9.50	32.18	7.99	2.24	3.43	48.54
11.00	33.34	5.90	1.87	3.27	47.15
landslide profile B63-4					
3.00	24.60	12.09	1.96	3.31	42.52
4.50	24.80	11.11	2.92	3.38	44.15
5.00	29.52	11.20	2.51	3.31	55.26
5.50	24.10	11.48	3.65	2.49	64.91
8.00	30.71	7.68	2.82	3.47	47.21
10.50	33.05	8.74	2.50	3.47	51.38
12.50	36.12	6.88	3.14	3.58	52.95

The clay fraction samples are composed mainly of smectite with subordinate amount of illite and kaolin minerals (Fig. 15). Because illite and kaolin minerals have almost none of the ion exchange properties (Matsuo *et al.*, 1979), the exchangeable cation contents and CECs in the clay fraction samples are attributed chiefly to smectite. Therefore, the exchangeable cation contents and CECs of smectite from the landslide profiles can be calculated based on the exchangeable cation contents and CECs of the clay fraction samples by normalizing the relative abundance of smectite in the clay fraction samples (Fig. 15), and the results are shown in Figs. 19 and 20. As is evident in the two figures, smectite from the landslide profiles of $A63-2$ and $B63-4$ is characterized by the presence of the predominant exchangeable Ca^{2+}, indicating Ca-smectite. Near the slip zone, Na^{+} is considerably absorbed in smectite, whereas Ca^{2+} concentration decreases, suggesting the presence of Na-smectite (Matsuo *et al.*, 1979). CECs of smectite from the landslide profiles of $A63-2$ and $B63-4$ are high values of 76.6 and 78.4 $meq/100g$ on the average, respectively, and increase to 91.1 and 90.0 $meq/100g$ near the slip zone.

C. Chemical analysis

The results obtained are tabulated in Tables 4 and 5 for the bulk and the clay fraction samples, respectively. The results are also shown graphically in Figs. 21 and 22. No systematic variation of chemical composition with the depth is recognized in the two landslide profiles.

Table 4. Chemical compositions of the bulk samples.

Depth	TiO_2	Al_2O_3	Fe_2O_3	MnO	MgO	CaO	Na_2O	K_2O
m	wt.%	wt.%	wt.%	wt.%	wt.%	wt.%	wt.%	wt.%
landslide profile A63-2								
1.00	0.48	14.28	1.97	0.034	0.31	0.82	0.29	3.91
1.50	0.26	12.98	1.21	0.018	0.26	0.34	1.53	3.45
2.00	0.25	10.04	0.63	0.010	0.14	0.26	1.40	2.98
2.50	0.26	9.16	0.63	0.008	0.14	0.26	1.37	2.90
3.00	0.29	10.27	0.62	0.009	0.14	0.25	1.41	3.26
3.50	0.24	10.05	0.72	0.013	0.15	0.28	1.45	3.27
4.00	0.23	10.90	2.87	0.046	0.15	0.28	1.74	3.17
4.50	0.27	10.51	6.00	0.020	0.14	0.25	1.55	3.01
5.00	0.54	18.83	4.68	0.020	0.72	0.87	0.28	2.64
5.50	0.63	17.99	4.54	0.021	0.75	0.86	0.33	2.66
6.00	0.56	18.19	4.64	0.018	0.70	0.88	0.38	2.74
6.50	0.52	17.52	4.81	0.020	0.73	0.87	0.36	2.68
7.00	0.53	17.44	5.00	0.021	0.72	0.88	0.38	2.72
7.50	0.52	17.87	4.85	0.019	0.70	0.87	0.38	2.74
8.00	0.49	17.43	5.03	0.023	0.73	0.94	0.76	2.49
8.50	0.47	14.38	2.74	0.017	0.71	0.85	1.12	2.57
9.00	0.56	17.21	4.86	0.026	0.74	0.99	1.38	2.38
9.50	0.45	17.39	5.37	0.030	0.79	1.16	1.28	2.26
10.00	0.51	16.85	5.12	0.028	0.75	1.10	1.34	2.38
10.50	0.50	15.75	5.91	0.029	0.72	0.97	1.37	2.60
11.00	0.59	17.73	5.31	0.028	0.74	0.88	0.96	2.52
landslide profile B63-4								
1.00	0.46	16.92	6.90	0.015	0.56	0.33	0.26	2.28
1.50	0.53	16.80	6.33	0.016	0.56	0.33	0.38	2.41
2.00	0.55	15.58	4.59	0.032	0.58	0.31	0.37	2.34
2.50	0.55	16.23	4.44	0.015	0.63	0.47	0.57	2.54
3.00	0.50	16.39	4.50	0.015	0.64	0.49	0.50	2.45
3.50	0.49	16.08	4.34	0.016	0.62	0.56	0.57	2.30
4.00	0.46	16.04	4.17	0.020	0.61	0.52	0.67	2.45
4.50	0.46	14.47	2.97	0.026	0.49	0.49	1.32	2.81
5.00	0.39	13.88	1.70	0.017	0.39	0.61	1.79	3.19
5.50	0.51	16.55	4.58	0.015	0.62	0.55	0.58	2.57
6.00	0.44	15.44	4.54	0.028	0.56	0.62	1.05	2.53
6.50	0.54	17.09	4.76	0.022	0.69	0.70	0.92	2.36
7.00	0.56	16.67	5.25	0.030	0.79	0.90	1.39	2.73
7.50	0.57	16.66	4.42	0.025	0.78	0.87	1.31	2.80
8.00	0.60	16.27	4.47	0.024	0.47	0.87	1.42	2.82
8.50	0.49	16.14	5.64	0.027	0.77	0.89	1.44	2.65
9.00	0.53	16.60	4.71	0.028	0.76	0.89	1.49	2.61
9.50	0.55	16.08	4.76	0.029	0.76	0.92	1.45	2.57
10.00	0.65	18.82	3.46	0.033	0.77	0.98	1.10	2.16
10.50	0.55	18.25	5.43	0.043	1.00	1.18	0.70	1.91
11.00	0.57	15.92	5.12	0.033	0.70	0.92	1.40	2.47
11.50	0.58	15.07	3.96	0.027	0.62	0.93	1.76	2.59
12.00	0.55	15.77	3.55	0.026	0.69	0.97	1.78	2.70
12.50	0.59	16.19	4.69	0.030	0.73	0.99	1.68	2.62

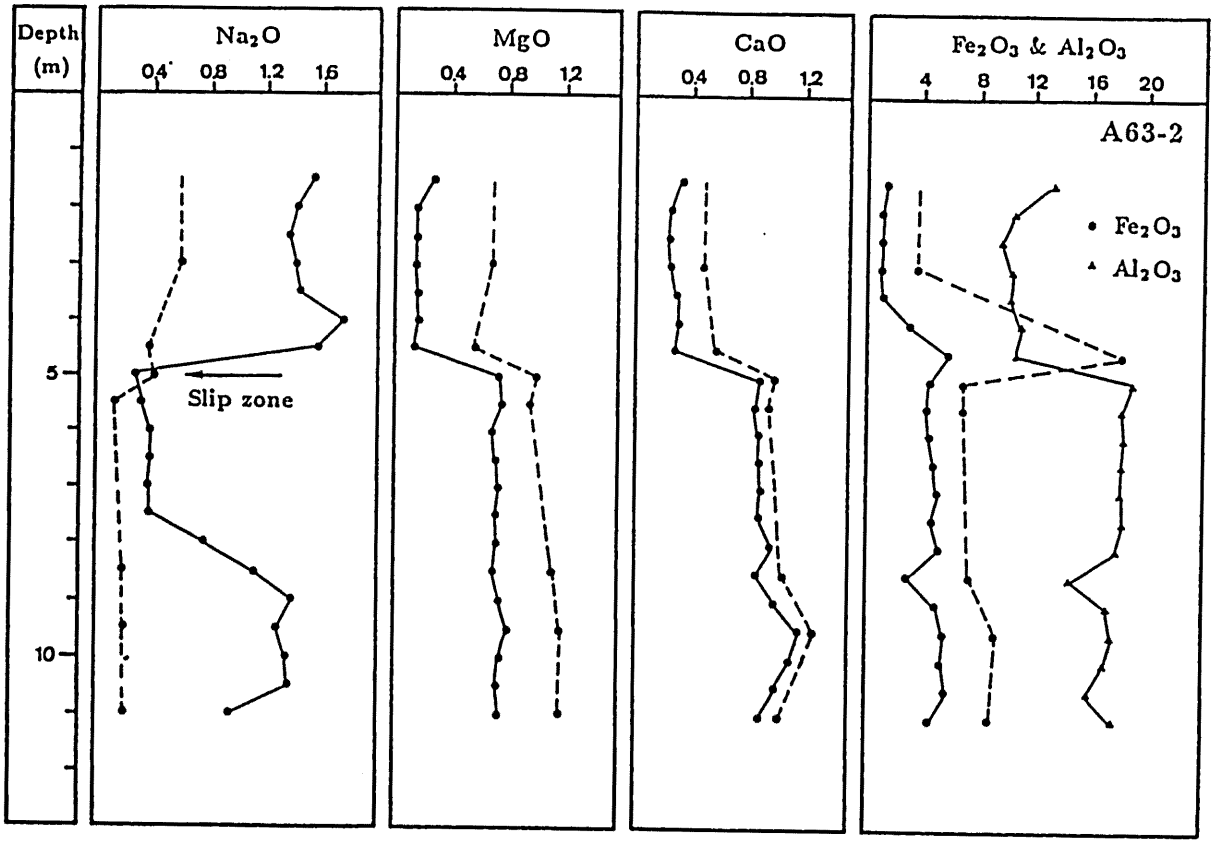

Fig. 21. Variation of chemical compositions with depth in the landslide profile A63-2. Solid line: bulk samples, broken line: clay fraction samples.

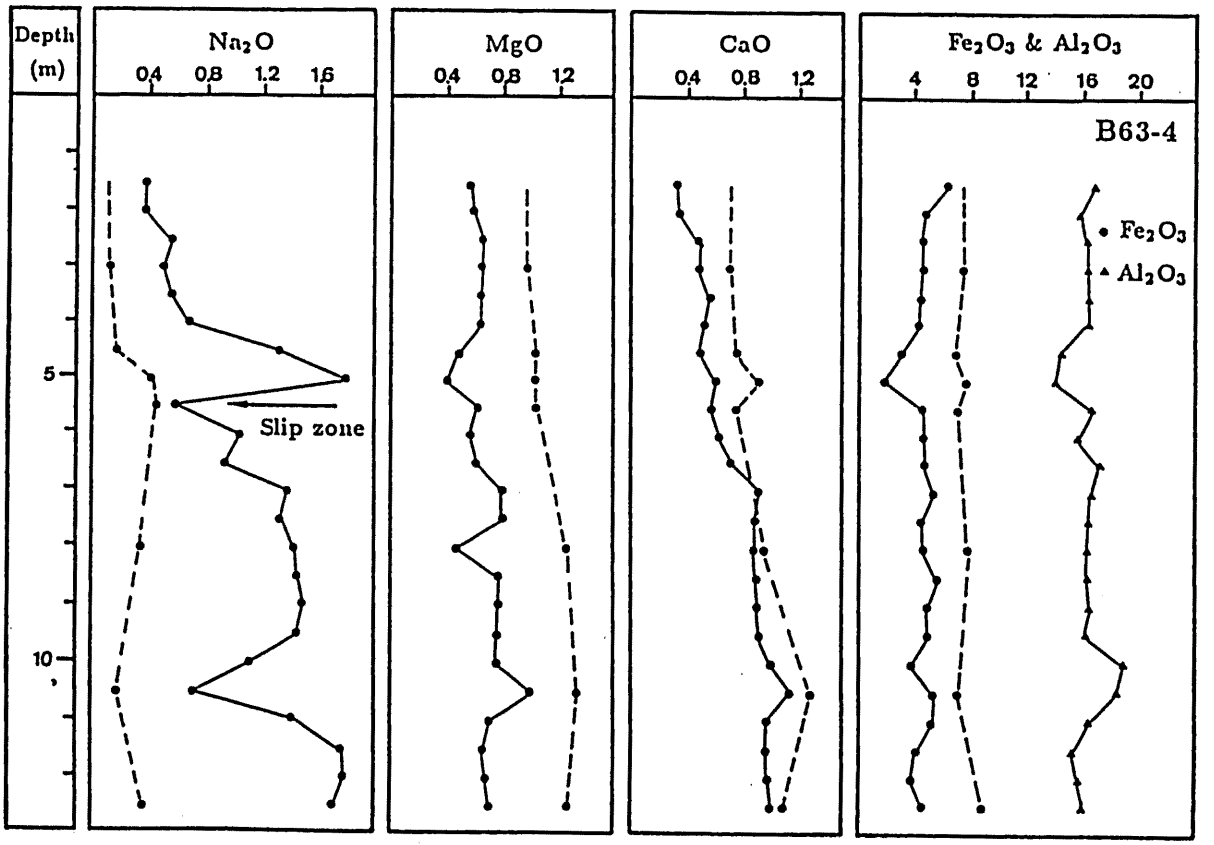

Fig. 22. Variation of chemical compositions with depth in the landslide profile B63-4. Solid line: bulk samples, broken line: clay fraction samples.

Table 5. Chemical compositions of the clay fractions.

Depth m	TiO_2 wt.%	Al_2O_3 wt.%	Fe_2O_3 wt.%	MnO wt.%	MgO wt.%	CaO wt.%	Na_2O wt.%	K_2O wt.%
landslide profile A63-2								
3.00	0.27	28.56	3.14	0.030	0.69	0.46	0.62	3.89
4.50	0.36	21.48	18.0	0.050	0.51	0.52	0.38	2.56
5.00	0.43	25.09	6.65	0.020	0.98	0.94	0.39	2.52
5.50	0.45	25.26	6.61	0.020	0.94	0.87	0.44	2.47
8.50	0.52	23.54	7.23	0.031	1.08	0.97	0.11	2.43
9.50	0.41	22.28	9.47	0.046	1.17	1.24	0.20	1.30
11.00	0.54	26.05	8.56	0.037	1.15	1.02	0.21	2.21
landslide profile B63-4								
3.00	0.47	22.96	7.54	0.020	0.96	0.70	0.12	2.22
4.50	0.57	23.74	6.81	0.030	1.03	0.75	0.26	2.52
5.00	0.55	22.76	7.61	0.028	1.02	0.87	0.40	2.50
5.50	0.54	25.73	7.34	0.022	1.01	0.69	0.43	2.53
8.00	0.52	24.42	7.80	0.035	1.25	0.91	0.25	2.79
10.50	0.64	23.75	7.01	0.053	1.31	1.26	0.16	1.34
12.50	0.44	21.50	8.86	0.041	1.24	1.11	0.26	2.14

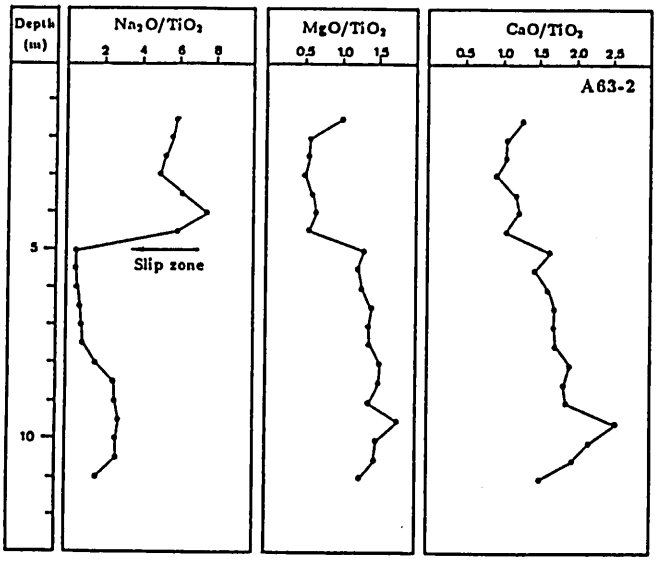

Fig. 23. Variation in ratios of Na_2O, MgO and CaO to TiO_2, respectively with depth in the landslide profile A63-2.

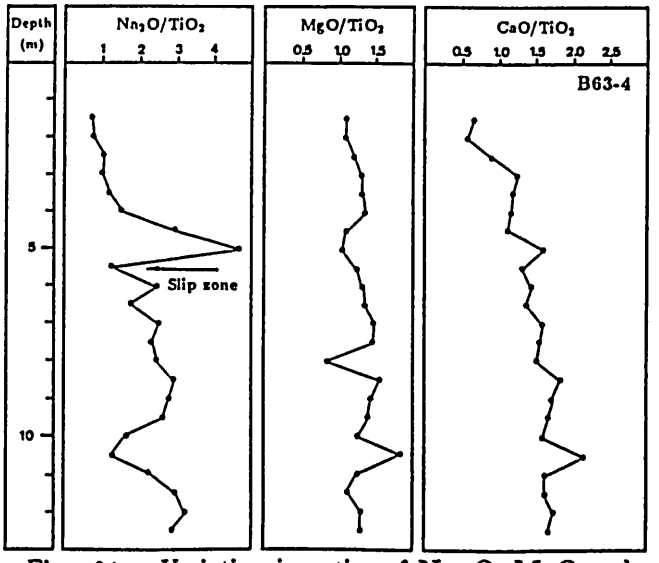

Fig. 24. Variation in ratios of Na_2O, MgO and CaO to TiO_2, respectively with depth in the landslide profile B63-4.

The variation of chemical composition for the bulk samples (solid line) with depth is similar to that determined for the clay fraction samples (broken line) in the profiles $A63-2$ and $B63-4$ (Figs. 21 and 22). CaO and MgO contents in the bulk and the clay fraction samples increase with depth in the two profiles, and Na content inversely decreases. Fe_2O_3 is highly concentrated just above the slip zone especially in the clay fraction samples (broken line) in the landslide profile $A63-2$ (Fig. 21), whereas the variation of iron concentration in the landslide profile $B63-4$ is relatively small (Fig. 22). The heavy metal titanium shows less variation with depth in the two landslide profiles (Tables 4 and 5). Ratios of MgO to TiO_2 and CaO to TiO_2 tend to increase with depth in the two profiles, whereas ratio of Na_2O to TiO_2 varies sharply, especially near the slip zone (Figs. 23 and 24). Ratio of Na_2O to CaO greatly increases just above the slip zone (Fig. 25).

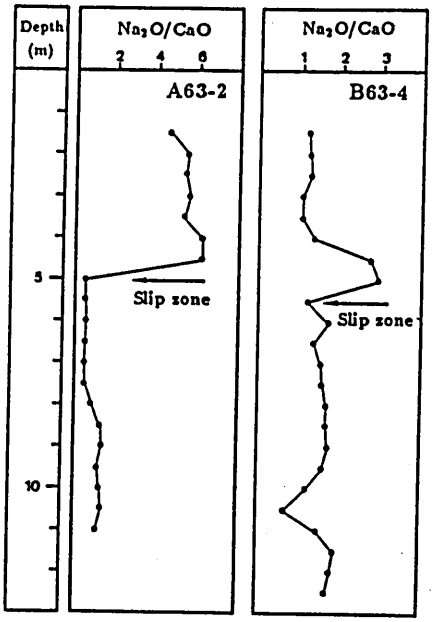

Fig. 25. Variation in ratio of Na_2O to CaO with depth in the landslide profiles of A63-2 and B63-4.

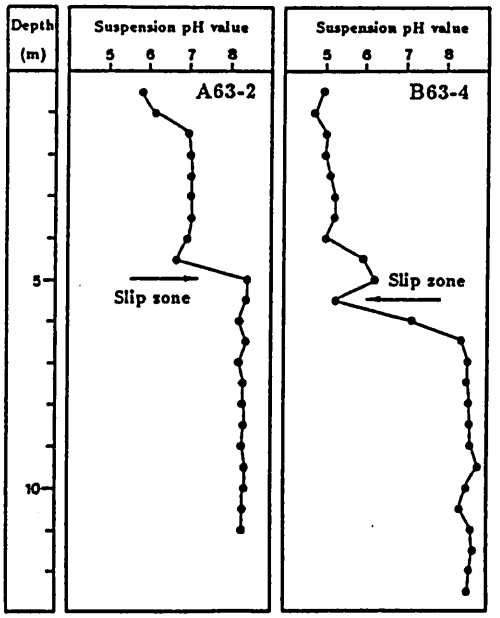

Fig. 26. Change of suspension pH against depth in the landslide profiles of A63-2 and B63-4.

D. Suspension pH value

Suspension pH values for the landslide materials from the landslide profiles $A63-2$ and $B63-4$ are illustrated in Fig. 26. As is evident in the figure, distinct difference in suspension pH values above and below the slip zone is recognizable. That is, above the slip zone the pH value is less than 7, and beneath the slip zone the value exceeds more than 8. The pH value varies sharply near the slip zone.

E. Groundwater chemical analysis

Groundwater analyses are compiled in Table 6. Samples of $a1$, $a2$ and $c1$ collected from the surface water near the toe of the landslide blocks show higher concentrations of Ca^{2+} and Mg^{2+}, whereas those of $a3$, $a5$, $a6$ and $c3$, collected also from the surface water in the neighboring area of the sliding head, are relatively lower. Samples of $a4$ and $c2$ are collected from drain borehole in contact with the slip zone, and show high Na^{+} and SO_4^{2-} concentrations.

Table 6. Chemical characteristics of groundwater.

No.	sampling location	pH	Ca^{2+} ppm	Mg^{2+} ppm	Na^{+} ppm	K^{+} ppm	SO_4^{2-} ppm
a1	surface water	7.39	11.28	3.71	10.20	5.97	27.50
a2	surface water	7.49	12.08	4.54	10.86	6.52	22.00
a3	surface water	7.52	12.36	4.35	10.33	6.15	17.00
a4	drain borehole	7.34	8.86	5.55	20.05	2.95	27.00
a5	surface water	7.64	13.48	4.52	8.20	6.64	15.50
a6	surface water	7.49	9.65	4.27	6.95	6.76	24.00
c1	surface water	7.38	15.33	5.60	10.00	6.17	21.00
c2	drain borehole	6.91	4.87	5.65	19.91	4.91	28.00
c3	surface water	7.17	2.64	0.78	1.42	3.86	N.D.

U.D. : not determined

The results are graphically illustrated in Figs. 27 and 28. The hydrochemical facies analysis shows that the surface water (black circle) in the landslide area is $Ca-Na$ type, and the groundwater (open circle) is $Na-Ca$ type (Fig. 27). The surface and ground waters can be distinguished clearly by chemical compositions (Fig. 28).

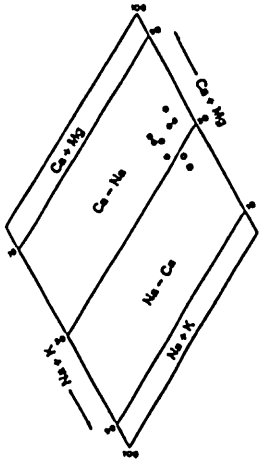

Fig. 27. Hydrochemical facies diagram of ground and surface water at Monden landslide area.
Open circle: groundwater, black circle: surface water.

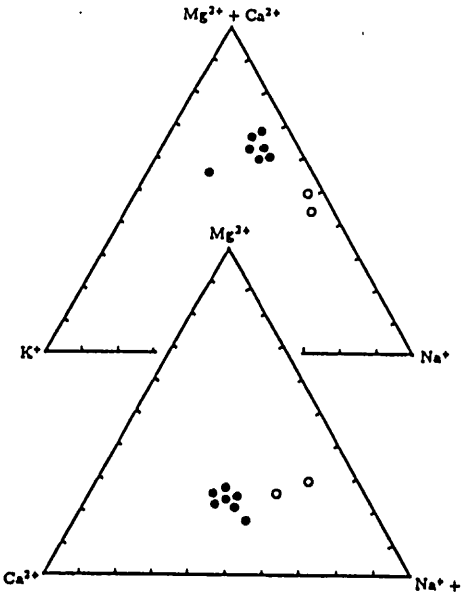

Fig. 28. Trilinear diagram of cations in groundwater at Monden landslide area.
Open circle: groundwater, black circle: surface water.

F. SEM observation

Landslide profile A63-2 Several distinctive clay particle aggregations with different degrees of preferred orientation were identified in undisturbed samples from the landslide profile $A63-2$. One aggregation type is skeletal-matrix texture with high porosity (Plates 1A and C). In the texture pattern, coarse particles float in a matrix of flaky clays. Porosity is high, and most pores have a diameter of 1 to 2 μm. Large pores are rare, mostly occurring between grain-grain contacts of coarse particles. The clusters (floc) are slightly predominant in the texture. A higher magnification picture (Plate 1B) shows that the clusters are composed of randomly oriented clay particles with low to high angle edge-face (EF) contacts. More rarely, face-face (FF) and edge-edge (EE) contacts occur within the clusters. Some hexagonal shaped clay flakes comprising the clusters (Plate 1B) obviously represents illite or kaolin minerals (Borst and Keller, 1969; Keller, 1976).

A second aggregation type is a highly parallel particle orientation with nearly perfect FF contact (Plates 2B, C and D), and this type is observed mostly in the landslide clays. The aggregation has poorly-defined outer boundary of the individual clay particles. The clay particles within the clusters are very thin and have wave-like edges (Plates 2B and D), indicating smectite (Borst and Keller, 1969; Keller *et al.*, 1986). The clay packing is dense, FF clay particle contacts dominate with rare occurrence of low angle EF particle contacts. Some packages are so densely welded together that the individual clay particles can not be discerned (Plate 2C).

Another aggregation type is a typical flocculent texture (Plates 3 and 4), having approximately equal amount of E and FF particle contacts. A higher magnification view (Plate 3B) shows that the clay particles have smooth surface and wave-like outer boundary. The cornflake or cellular appearance of the clay particles indicates that the

clays in Plates 3 and 4 are smectite (Baracos, 1984; Keller *et al.*, 1986). The flocculent texture was frequently observed mainly in undisturbed samples below the slip zone, presumably due to the increase of smectite (see XRD analysis section).

Additionally, a coating of fine-granule material on the surface of the clay particles (Plate 1D) was occasionally observable in samples of 30 to 45 *cm* depths. It is of interest that in the landslide clay, occasionally, sliding cast and slickenslide were observed parallel to the slip zone (Plate 2A).

Landslide profile B63-4 Aggregation characteristics observed in the landslide profile $B63-4$ are similar to those displayed in the landslide profile $A63-2$, including skeletal-matrix aggregation (Plates 5 and 6), a strongly parallel particle orientation with perfect FF particle contacts (Plates 7A and C) and flocculent pattern (Plate 8). It is noteworthy that the landslide clay parallel to the slip zone shows highly oriented FF contact texture (Plates 7A and C). Texture patterns away from the slip zone or perpendicular to the slip zone are characterized by randomly oriented particle contacts (Plate 7D). In addition, a slickenslide (Plate 7B), due presumably to sliding, was also observed in the landslide clays from the landslide profile *B*.

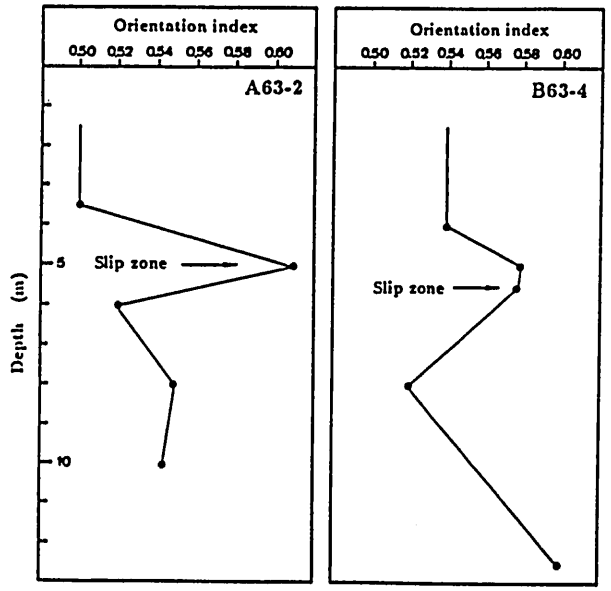

Fig. 29. Variation of orientation index with depth in the landslide profiles A63-2 and B63-4.

Special attention should be given to particle reorientation. The shearing processes can cause the changes in clay particle contacts. The particle reorientation reflected in clay aggregation provides clues on the postdepositional mechanical processes. During direct simple shear testing of the landslide clays, a large number of well-aligned zones of densified clay particles and clusters were formed along shearing failure plane (Plates 9C and D) and the matrix (clay particles) comprising the cluster has been reoriented into high degree of alignment with perfect FF particle contacts (Plate 9D). On the other hand, away from the shearing plane or in the surface normal to shearing stress, most aggregation patterns are unchanged from its original appearance (Plates 9A and D). Obviously, SEM observation of the sheared samples shows that the particle preferred orientation occurs as a result of shearing deformation. The sheared samples display FF particle contacts with fairly-developed particle orientation similar to that observed in the landslide clays.

Particle orientation Fig. 29 shows the orientation index in terms of intensity of the basal reflection of smectite for the two landslide profiles. As is evident in Fig. 29, the orientation index greatly increases toward the slip zones. In the landslide profile *B*, the sample of 12.0 *m* depth shows high orientation index.

G. Rheological behavior of remoulded kaolin sample

Fig. 30 shows the displacement versus time curves for set 1 and set 2. As is seen in this figure, the water pressure has little influence on the creep displacement at low shearing stress levels (open circle and open triangle), but the displacement increases more and more with increasing shearing stress (black circle and x mark).

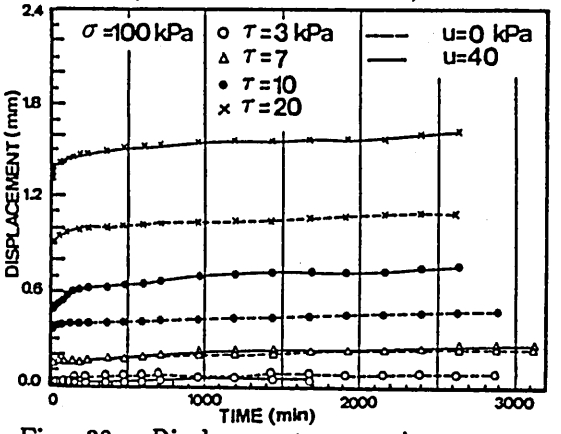

Fig. 30. Displacement versus time curves for remoulded kaolin samples.

Fig. 31 presents the displacement versus time curves for set 3. In this test, when the water pressure increases to 80 *kPa*, the displacement rate (slope of displacement versus time) increases rapidly and creep failure occurs. The changes in the pore water pressure during creep deformation are shown in Fig. 32. At steady stage, the pore water pressure occurring in samples is equal to the applied water pressure, however, it tends to decrease at failure (x mark).

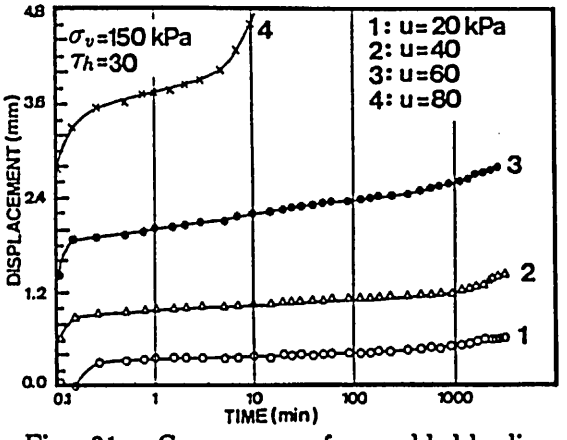

Fig. 31. Creep curves of remoulded kaolin samples.

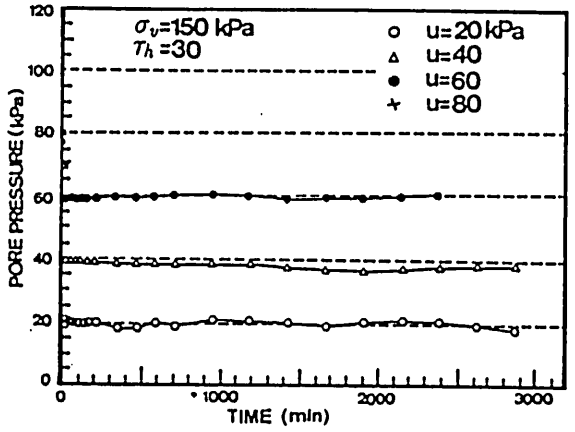

Fig. 32. Changes of pore water pressure during creep deformation.

Fig. 33 shows the pore water pressure versus displacement rate calculated according to the slope of the displacement versus time curve at steady stage. As is clear in the figure, the pore water pressure largely influence the creep displacement rate.

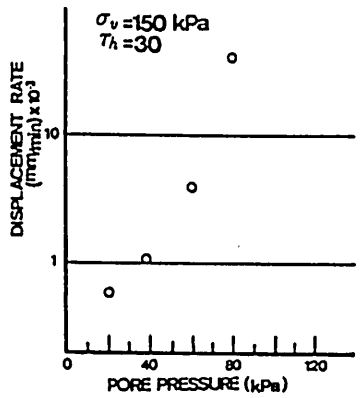

Fig. 33. Relation of displacement rate and pore water pressure.

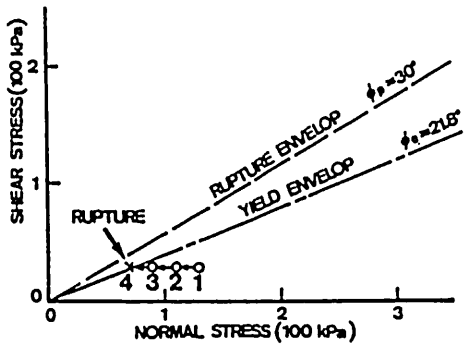

Fig. 34. Creep failure attributed to the increase of pore water pressure.

To understand the phenomenology of creep failure, the results are plotted as the function of the vertical stress and the shearing stress (Fig. 34). In Fig. 34, the rupture envelop line ($\phi p = 30°$) and the yield envelop line ($\phi c = 21.8°$) were determined based on the results of triaxial compression consolidated-drained test and direct shearing test, respectively (Nakamori *et al.*, 1993). As shown in this figure, the increase in the pore water pressure causes the decrease of the effective stress (from test 1 to test 4), which in turn leads to the increase of the creep displacement rate, resulting finally the creep failure (arrow).

H. Rheological behavior of Monden landslide clay

The results of the three direct simple shear tests for the landslide clays are shown in Figs. 35 and 36. The pore water pressure is almost equal to the applied water pressure, and remains unchanged during shearing deformation (Fig. 35). The larger the pore water pressure, the higher the creep displacement rate. The creep displacement rate increases with increasing the pore water pressure (Fig. 36). The effect of the pore water pressure on the creep displacement rate in the landslide clay is similar to that in the remoulded kaolin samples.

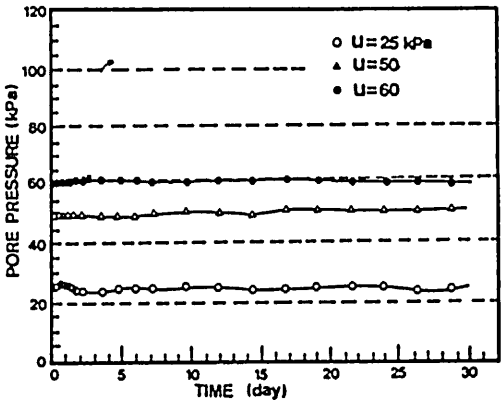

Fig. 35. Change of pore water pressure during creep deformation for the Monden landslide clays.

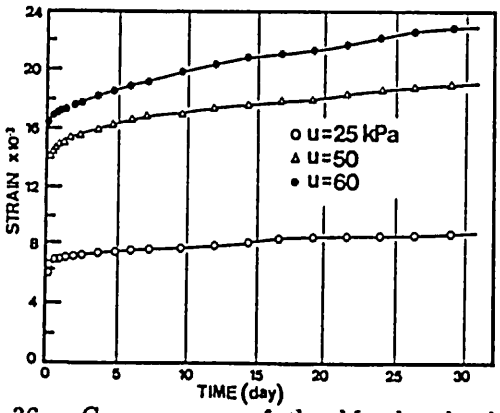

Fig. 36. Creep curves of the Monden landslide clays.

VI. Discussion

The landslide in the Monden area is characterized by slow creep movement at the rate of 2 to 10 *cm* per year (Fig. 7) and can be considered as a typical creeping landslide. In the following, occurrence mechanism of landslide related to the internal factors and deformation characteristics of clay sediments will be discussed.

1. Mechanism of creeping landslide

Based on the inclinometer measurement and boring core observation, a sharply defined slip zone of about 0.5

m in thickness was recognized in the Monden landslide area. In the landslide profile of $A63-2$, the slip zone is located at depths of about 4.5 to 5.0 m, and in the landslide profile of $B63-4$ at 5.0 to 5.5 m depth, respectively.

In the two profiles, smectite is the main constituent clay mineral, and smectite content tends to increase toward the slip zone. Furthermore, mineralogical properties of smectite abruptly change near the slip zone. Near the slip zone, the expandability of smectite at 100% relative humidity is low, the CEC value is high and the ratio of Na^+ to Ca^{2+} in the interlayer is extremely large. Chemical analysis of the bulk samples clearly represents high ratio of Na_2O/CaO above the slip zone. Suspension pH values abruptly increase just beneath the slip zone. In addition, aggregation characteristics and particle orientation of the landslide material are different between above and beneath the slip zones. That is, porous skeletal-matrix aggregation type and flocculent aggregation type are characteristic. The landslide clays of the slip zone itself (landslide materials in the slip zone) show, however, highly oriented face-face contact type with high particle orientation.

Based on mineralogical and aggregation texture characteristics of the landslide materials, the landslide profiles are divided into three zones, *i.e.*, upper zone, slip zone and lower zone. Color of the materials of the three zones is different with each other; the upper zone is brown, the slip zone blackish gray and the lower zone light green. At the lower part of the upper zone, iron is highly concentrated (Figs. 21 and 22), and values of suspension pH abruptly increase. The upper zone is characterized by oxidation state. In relation to this, the flow surface of groundwater is situated near the slip zone. The materials of the upper zone show skeletal-matrix aggregation with high porosity, and thus have comparatively high permeability, indicating that the materials tend easily oxidized because the zone is in contact with air containing much O_2 and CO_2 (Reynolds and Johnson, 1972).

Role of groundwater is of significance on the activity of chemical weathering (Isagai *et al.*, 1987; Shuzui and Kawahara, 1987). As was pointed out by Isagai *et al.* (1987), chemical weathering is active when the groundwater contains large amount of ions, such as bicarbonate, sulfate, calcium and so on. Under these circumstance, occurrence of landslide is common. In the Monden landslide area, high SO_4^{2-} concentration in groundwater is recognized (Table 6). This is probably ascribed to oxidation of pyrite (Magaritz and Luzier, 1985). Thus the decomposition of the landslide materials of the district was proceeded remarkably (Ando, 1976; Vear and Curtis, 1981). The content of feldspar in the landslide materials tends to decrease toward the slip zone from the upper zone (Figs. 13 and 14) and on the other hand, Ca and Mg content in smectite gradually increase with depth (Figs. 21 and 22). The variations in ratios of MgO and CaO to TiO_2 with depth (Figs. 23 and 24) are similar to the distribution pattern of smectite in the two landslide profiles (Fig. 15). As is clear in Fig. 15, smectite content near the slip zone is large and the composition of smectite is characterized by high Mg and Ca contents (Ojanuga, 1979).

Suspension pH value is almost equivalent to the H ion activities around mineral grains. The low pH values of the upper zone can be explained by the exchange reaction of H^+ for cations such as Na^+, Ca^{2+} and Mg^{2+} derived from clay minerals, especially smectite. These reactions cause high pH values (Fig. 26). Furthermore, the migration of groundwater together with surface water dissolves primary minerals such as feldspar. Thus, the groundwater in the landslide area has high cation concentrations such as Ca^{2+}, Mg^{2+} and Na^+, and exchanges the cations of smectite. Among these cations, Ca^{2+}, Mg^{2+} and Na^+ occupy the interlayer position.

Figs. 19 and 20 show the exchangeable cation contents and the CECs of smectite from the landslide materials. As is seen in the figures, Ca^{2+} and Mg^{2+} are the most dominant exchangeable cations. At certain depths, especially near the slip zone, exchange of Na^+ is characteristic. Considering valency, Na^+ is readily replaced by Ca^{2+} and Mg^{2+}. However, Na ion in smectite, when present in sufficient amount in groundwater, could easily replace Ca^{2+} and Mg^{2+}. The ratio of Na_2O to CaO sharply increases above the slip zone (Fig. 25) indicating the presence of high Na ion source. Therefore, the following alteration sequence of smectite is suggested at certain depths, especially near the slip zone:

(Ca, Mg) smectite $+ Na^+ \rightarrow (Ca, Mg, Na)$ smectite $+ (Ca^{2+} + Mg^{2+})$, or

(Ca, Mg) smectite $+ Na^+ \rightarrow Na$-smectite $+ (Ca^{2+} + Mg^{2+})$.

The term *clay texture* denotes, in general, the geometric arrangement of the constituent mineral particles and void space (Kezdi, 1974; Yong and Warkentin, 1975). Key terms such as face-face (FF) contact, edge-face (EF) contact, edge-edge (EE) contact and so on are commonly employed in the description and discussion of clay texture, and will be used in this paper according to Yong and Warkentin (1975) and Gillott (1987). As described in the previous, in the landslide materials, three distinctive aggregation types (three texture patterns) are confirmed. That is, skeletal-matrix texture, parallel particle orientation with perfect FF contact and flocculent texture. The skeletal-matrix texture is observed mostly in samples in the upper zone. In general, each clay mineral has its own grain shape and forms characteristic particle arrangement. The clay fractions in the upper zone are composed mainly of illite and kaolin minerals, therefore, the clay texture of the upper zone is characterized by open particle arrangement with high porosity. The porous skeletal-matrix texture is favorable for migration of groundwater and surface water, and thus liable to leaching and dissolution of minerals. Fine-granule materials observed in the upper zone are usually coated by thin films and the films were presumably the results of precipitation of dissolution products.

The highly oriented parallel FF particle contact pattern is observed in the slip zone in which smectite is abundant. The texture is very similar to that displayed in tested samples by direct simple shear apparatus. Furthermore, sliding cast and slickenside are occasionally observed parallel to the slip zone. Therefore, the development of high orientation with FF particle contact is attributed to the

gravitational creep or sliding processes. Smectite particle is very thin and pliable, and is easily reoriented (Muller-Vonmoos and Loken, 1989). Therefore, the smectite-dominated landslide materials of the slip zone are readily welded densely and become more impermeable under certain shearing or compression conditions (Plates 2B, 2D and 7A). Furthermore, reorientation of platy clay minerals decreases the undrained shear strength of the materials to the residual strength (Skempton, 1985). Moreover, the highly oriented FF particle contacts clearly indicate weak inter-particle bonding by thin water films. This is because of high water absorption capacity of smectite, and the fact promotes the readily break and reform nature of the mineral. The texture is particularly significant for the start of creep movement.

The flocculent texture is a typical aggregate pattern of smectite-rich clays (Yong, 1971), and is observed mainly in undisturbed samples below the slip zone. The texture easily changes to highly oriented FF contact texture under shearing condition as stated above, The clay texture found in sheared samples evidently indicates that the shearing processes affect the clay texture and a typical example is the change of reorientating high-angle EF contacts to low-angle contacts to FF contacts. Therefore, the highly oriented FF contact texture observed in the slip zone are probably resulted by the rearrangement of the flocculent texture under shearing processes.

It is well known that in Tertiary formation landslide areas, smectite is frequently recognized as major constituent mineral, and landslide occurrence depends largely on smectite content because of its unique physicochemical properties (Shuzui, 1984; 1986; Maeda and Fukuda, 1991). Smectite has various and large amount of exchangeable interlayer cations and the cations are commonly hydratable (Odom, 1984; Moore and Hower, 1986). Therefore, smectite shows high hydration and swelling properties (Matsuo and Tomita, 1970; Iwasaki and Watanabe, 1988). The degree of swelling (expandability) depends on the species (size and charge) and amount of exchangeable cations (Odom, 1984). When Na^+ is the dominant exchangeable cation, smectite shows a high expandability. Na^+ in smectite increases amount of interlayer water until complete dissociation of the smectite crystals in the extremely case. On the other hand, smectite containing exchangeable Ca^{2+} and Mg^{2+} swells only a small degree even when fully hydrated (Odom, 1984). Based on X-ray diffraction analysis, *Na*-smectite is proved to be more expandable than *Ca*-smectite or *Mg*-smectite with increasing relative humidity (Watanabe and Sato, 1988). Moore (1985; 1991) experimentally clarified that smectite saturated with *Na* cations consistently has lower residual strength than that saturated with *Ca* or *Mg* cations.

As mentioned above, because the smectite-rich landslide materials in the slip zone has little permeability, the cations such as Ca^{2+}, Mg^{2+} and Na^+ are easily encountered with the landslide materials and exchange reaction of Ca^{2+} and Mg^{2+} for Na^+ extensively takes place. As shown in Fig. 37, the decrease in mechanical strength (N-value) is caused mostly by the exchange of Ca^{2+} and Mg^{2+} for Na^{2+}. Therefore, the exchange of Ca^{2+} and Mg^{2+} for Na^{2+} is of important clay mineral alteration in relation to landslide occurrence. The reaction in turn greatly promotes the hydration and expandability of smectite causing the decrease of mechanical strength of the soils and the formation of highly lubricant landslide materials with low mechanical strength.

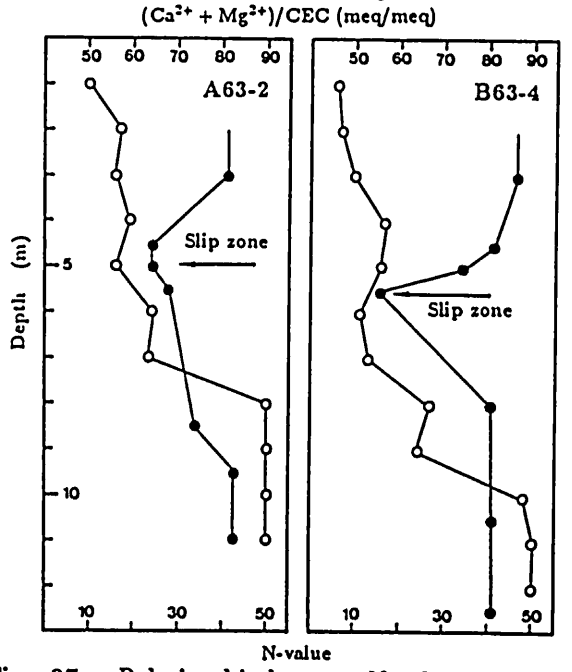

Fig. 37. Relationship between N-value and the ratio of $(Ca^{2+} + Mg^{2+})$ to CECs in the landslide profiles of A63-2 and 63-4. Open circle: N-value, black circle: $(Ca^{2+} + Mg^{2+})/CEC$.

2. Prediction of landslide deformation

In this section, first a slope model is established based on the morphological characteristics and mechanism of the creeping landslide and then fundamental equations are introduced to explain the time-dependent deformation behavior of the landslide clays. Based on the equations, prediction is then made using parameters obtained through in situ observation such as groundwater levels. The predicted displacements will be compared with actual data. The comparison will confirm whether the constitutive equations are effective in predicting the deformation in the creeping landslide or not.

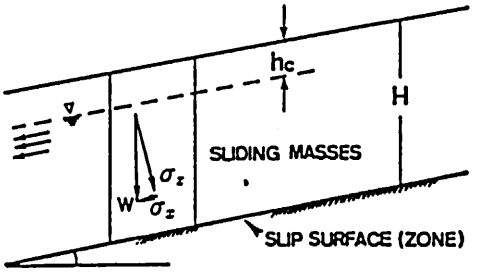

Fig. 38. Slope model. H: height of slip zone, h_C: height of groundwater level, σ_z: vertical stress, σ_x: horizontal stress, W: gravitational force.

As already stated, the Monden landslides occur along

long slope more than 400 m and characterized by slow creep movement. Slip zones almost parallel to geographical slope of about 10 degrees were recognized in the present research. Moreover, the displacement of the landslide greatly increases following heavy rainfall as shown in Fig. 7. The results of direct simple tests consistently the indicate that the higher pore water pressure always corresponds to the larger displacement rates. Therefore, an infinite long slope (Fig. 38) is assumed to consist of sliding mass and thin landslide clay layer (slip zone). To simplify the analysis, the slope is represented by a two-dimensional model. The deformation of the landslide is considered to be due to the hydrodynamic lag and the creep effects.

Based on the above slope model, the stress and strain spaces of the slip zone are given as follows:

$$\sigma_x \neq 0, \quad \sigma_y = 0, \quad \sigma_z \neq 0, \quad \varepsilon_x \neq 0, \quad \varepsilon_y = 0, \quad \varepsilon_z \neq 0$$

σ and ε are stress and strain, respectively and suffix x, y and z represent the respective direction.

The creeping landslide is a slowly sliding phenomenon of shallow soil layers as shown in Fig. 7, and can be considered to be as viscoelastic flow. Thus, the mechanical properties can be determined by the rheological model parameters illustrated in Fig. 39.

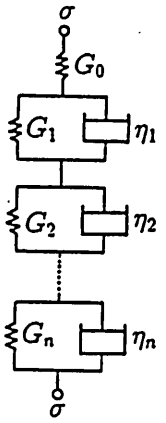

Fig. 39. Rheological model. σ: stress, G: shear modulus, η: coefficient of viscosity.

According to rheological rules (Sobotka, 1984), the stresses in all groups are the same:

$$\sigma = G_0\varepsilon_0 = G_1\varepsilon_1 + \eta_1\frac{d\varepsilon_1}{dt} = \ldots = G_n\varepsilon_n + \eta_n\frac{d\varepsilon_n}{dt} \quad (1)$$

On the other hand, the strains are added as expressed by the following strain-stress-time relation:

$$\varepsilon(t) = \sigma_0\left(\frac{1}{G_0} + \sum_{i=1}^{n}\frac{1}{G_i}\left(1 - e^{-\frac{G_i}{\eta_i}t}\right)\right) \quad (2)$$

Where

$$J_i = \frac{1}{G_i}, \quad T_i = \frac{1}{G_i}\eta_i, \quad J(t) = J_0 + \sum_{i=1}^{n} J_i\left(1 - e^{-\frac{t}{T_i}}\right)$$

Therefore, Eq. 2 can be simply expressed as follows:

$$\varepsilon(t) = \sigma_0 J(t) \quad (3)$$

If the stress is a continuous function of the retardation time λ $(0 < \lambda < t)$, the sum is replaced by an integral. The following integral equation is obtained (Akagi *et al.*, 1976):

$$\varepsilon(t) = J_0\sigma_0 + \int_0^t J(t-\lambda)\frac{d\sigma(\lambda)}{d\lambda}d\lambda \quad (4)$$

When the stress is constant and the number of the voigt groups tends to infinity, we have:

$$\varepsilon(t) = \sigma_0\left(J_0 + \int_0^\infty (1 - e^{-\frac{t}{\lambda}})\frac{dJ(\lambda)}{d\lambda}d\lambda\right) \quad (5)$$

where $J(\lambda)$ is a continuous function of the retardation time.

Introducing the following new function (the retardation spectrum):

$$\Phi(\lambda) = \lambda\frac{dJ(\lambda)}{d\lambda} \quad (6)$$

Eq. 5 becomes:

$$\varepsilon(t) = \sigma_0\left(J_0 + \int_0^\infty \Phi(\lambda)(1 - e^{-\frac{t}{\lambda}})d(\ln\lambda)\right) \quad (7)$$

From Eq. 7, when the deformation can be determined by classifying the retardation time λ and the number of voigt groups, the model parameters become physically and mechanically meaningful and, can be determined.

Differentiating Eq. 3 for t, and then substituting it into Eq. 6, the retardation spectrum is given as follows:

$$\Phi(\lambda) = \frac{\lambda}{\sigma_0}\frac{d\varepsilon}{d\lambda} \quad (8)$$

For the creep curves of the landslide clays (Fig. 36), the parameters of the constitutive equations are determined based on the spectral analysis as described by Akagi *et al.* (1976) and Akagi (1981; 1985) and given in Table 7.

Table 7. Rheological parameters of landslide clays.

τ_h kPa	T_1 day	T_2 day	J_1 $kPa^{-1} \times 10^{-6}$	J_2 $kPa^{-1} \times 10^{-6}$
19	2	9	13.67	3.96
18	2	6	11.07	2.11

The retardation time, T, is rather small, and is thus revised by using field measurement displacement. The revised retardation times, T_1 and T_2, are respectively 0.66×10^3 (month) and 3×10^3 (month) in $\tau_h = 19kPa$ case, and 0.66×10^3 (month) and 2×10^3 (month) in $\tau_h = 18kPa$ case.

The determined parameters are substituted into Eq. 3. The average slope length, L, is 400 m. Moreover, the instantaneous strain response should not be considered because the field measurement was carried out after landslide occurred.

Therefore, where τ_h is equal to 19 kPa, the horizontal displacement:

$$\Delta L(mm) = 103.87(1 - e^{-0.015t}) + 30.11(1 - e^{-0.0033t})$$

$(t : month)$,

and where τ_h is equal to 18 kPa,

$$\Delta L(mm) = 79.67(1 - e^{-0.015}) + 15.19(1 - e^{-0.005t})$$

$(t : month)$,

Fig. 40 shows the predicted displacements by using the above formulae (open symbol) and the actual displacements (black symbol) for inclinometer hole $A59-2$ (data from Public Works Office, Okayama Prefecture, 1990). It is evident from this figure that the agreement between the predicted and actual displacements is satisfactory, and thus the present model can be used to predict the deformational processes in the creeping landslide. Moreover, the pore water pressure (groundwater level) exerts a considerable influence on the displacements of the landslide. The bigger pore water pressure (higher groundwater level) corresponds to the larger displacements (open circle) and the smaller pore pressure (lower groundwater level) to the smaller displacements (open triangle). The findings provide a reasonable explanation for creeping landslide triggered by a slight rise in the groundwater level during rainy season.

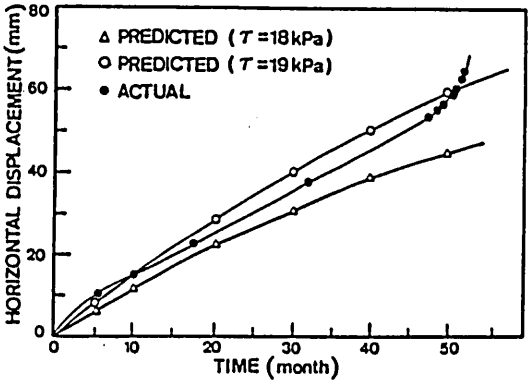

Fig. 40. Comparison of predicted and actual displacements.

As discussed above, the rheological model described by $\varepsilon(t) = \sigma J(t)$ or $\Delta L = \varepsilon(t)L$ can be used to predict the displacements of landslide. It should be kept in mind, however, that the parameter determination is based on the creep curve of small specimens over a short period of time and that the retardation time depends on the order of loading time. The retardation time determines the period of prediction. For example, let us consider the following creep function:

$$J(t) = J_0 + J_1(1 - e^{-\frac{t}{\tau_1}}) + J_2(1 - e^{-\frac{t}{\tau_2}}) + J_3(1 - e^{-\frac{t}{\tau_3}}) \quad (9)$$

Assuming that T_1 is minute, T_2 and T_3 are, respectively, day and year as the order of retardation times. If the time of loading is of the order of minute, Eq. 9 becomes:

$$J(t) = J_0 + J_1(1 - e^{-\frac{t}{\tau_1}}) \quad (10)$$

Similarly, if t is of the order of year, Eq. 9 can be approximately represented by the following equation:

$$J(t) = (J_0 + J_1 + J_2) + J_3(1 - e^{-\frac{t}{\tau_3}}) \quad (11)$$

This suggests that the period of prediction depends on the order of retardation time. Akagi *et al.* (1976) pointed out that the creep test method is suitable for obtaining the retardation times of more than a few seconds and smaller than a few decades. Therefore, further consideration on the retardation time should be performed.

VII. Summary and conclusions

Landslide occurring in the Monden area, Okayama Prefecture was investigated mainly from the viewpoint of mineralogy. Based on the obtained results, occurrence mechanism of the landslide was discussed taking into consideration of engineering soil constants. The results obtained can be summarized as follows:

1. The landslide of the Monden area moves slowly and continuously at the rate of 2 to 10 mm/yr, and the landslide is a creeping landslide.
2. The three zones, upper, slip and lower zones are distinguished based on the constituent clay minerals in the landslide profiles. The slip zone corresponds to the boundary between the upper and the lower zones.
3. Clays in the slip zone (landslide clays) are formed as a result of the shearing processes, and the clays are characterized by highly oriented FF contact texture and low mechanical strength.
4. Ca^{2+}, Mg^{2+} and Na^{+} were highly concentrated in the landslide materials of the slip zone and exchange of Ca^{2+} and Mg^{2+} for Na^{+} extremely took place in smectite, thus formed Na-smectite and/or (Na, Ca)-smectite are characterized by remarkable expandability. This characteristic feature decreases the mechanical strength and on the other hand, increases the lubricant capacity of the landslide materials.
5. The fluctuations of the groundwater levels exert a great influence on the displacements of the landslide zone. Taking the groundwater levels into consideration, a rheological model is presented in this study. Applying engineering soil constants determined in this study to the model, certain possibility for prediction of the deformational processes in the creeping landslide were confirmed. That is, the landslide occurrence during rainy season is reasonably explained by this model.

References

Akagi, T., Ito, Y. and Irobe, M. (1976): Viscoelastic analysis about the deformation of weak ground. *Proc. 1st Int. Conf. Num. Geomech.*, 639-649.

Akagi, T. (1982): Application of generalized rheological model to time-dependent behavior of rock. *Proc. 4th Int. Conf. Num. M. Geomech.*, 113-121.

Akagi, T. (1985): Application of rheological model to nonlinear creep properties of rock. *Proc. 5th Int. Conf. Num. M. Geomech.*, 415-421.

Ando, T. (1976): On weathering mechanism in landslides (in Japanese with English abstract). *Jour. Japan Landslide Soc.*, 26, 1-10.

Aramaki, S., Kitazono, Y., Suzuki, A. and Kajiwara, M. (1987): On physical properties of soils weathered from Tertiary sedimentary rock on Amakusa Island (in Japanese with English abstract). *Jour. Japan Soc. Eng. Geol.*, 28, 28-34.

Baracos, A. (1977): Composition and structural anisotropy of Winnipeg soil - a study based on scanning electron microscopy and X-ray diffraction analyses. *Can. Geotech. Jour.*, 14, 125-137.

Bennett, R. H., Bryant, W. R. and Keller, G. H. (1981): Clay fabric of selected submarine sediments - fundamental properties and models. *Jour. Sediment. Petrol.*, 51, 217-232.

Borst, R. H. and Keller, W. D. (1969): Scanning electron micrographs of API reference clay minerals and other selected samples. *Proc. Int. Clay Conf.*, 872-901.

Calvert, C. S., Buol, S. W. and Weed, S. B. (1980): Mineralogical characteristics and transformations of a vertical rock-saprolite-soil sequence in the north Carolina Piedmont - profile morphology, chemical composition and mineralogy. *Soil Sci. Soc. Am. Jour.*, 44, 1096-1103.

Chigira, M. (1987): Mechanism of chemical weathering of mudstone - weathering under the natural condition and slope stability (in Japanese with English abstract). *Rep. Central Res. Inst. Electric Power Industry*. 1-23.

Chigira, M. (1988): Chemical weathering of mudstone of the Pleistocene Haizume Formation, Niigata Prefecture, central Japan (in Japanese with English abstract). *Jour. Geol Soc. Japan*, 94, 419-431.

Chigira, M. (1990): A mechanism of the chemical weathering of mudstone a mountainous area. *Eng. Geol.*, 29, 119-138.

Delage, P. and Lefebver, G. (1984): Study of the structure of a sensitive Champlain Clay and of its evolution during consolidation. *Can. Geotech. Jour.*, 21, 21-35.

Fujimoto, H. (1967): Clay minerals in landslide masses from the west Japan (in Japanese). *Jour. Japan Landslide Soc.*, 9, 14-20.

George, F. S. and David, L. R. (1978): Field investigation, *Landslide analysis and control*, Schuster, R. L. and Krisek, R. J. Eds., Special report, 176, 81-11.

Gillott, J. E. (1987): Clay in engineering geology. Elservier, Amsterdam, 91-142.

Isagai, K., Isagai, K., Iwasaki, M. and Takagi, T. (1990): Distribution of chemical composition in groundwater by different type of landslides. *Jour. Japan Landslide Soc.*, 100, 16-28.

Isagai, K., Isagai, K., Imai, C. and Fujinaga, M. (1987): Chemical composition of groundwater in Ishikura landslide area in Nagasaki Prefecture - effect of amount of precipitation. *Jour. Japan Landslide Soc.*, 91, 30-40.

Iwasaki, T. and Watanabe, T. (1988): Distribution of Ca and Na ion diochtahedral smectite and interstratified diochtahedral mica/smectites, *Clays and Clay Minerals*, 36, 73-82.

Keller, W. D., Reynold, R. C. and Inoue, A. (1986): Morphology of clay minerals in the smectite to illite conversion series by scanning electron microscopy. *Clays and Clay Minerals*, 34, 187-197.

Koide, H. (1955): Landslides in Japan (in Japanese). *Toyo Keizai- shiposha*, 259.

Koide, H. (1962): Landslides in Japan (in Japanese). *Jour. Japan Soc. Civil Eng.*, 47, 12-19.

Koide, H. (1963): Landslide phenomenon and problems (in Japanese). *Science*, 33, 418-424.

Lupini, J. E., Shinner, A. E. and Vangham, P. R. (1981): The drained residual strength of cohesive soils. *Geotechnique*, 31, 181-213.

Maeda, H. (1988): Detritus and clay of slide horizon in the Ikutahara landslide, northeastern Hokkaido, Japan (in Japanese with English abstract). *Jour. Japan Landslide Soc.*, 93, 13-20.

Maeda, H. (1989): Geologic characteristics of recent landslides in the Ikutahara-Rubeshibe district, northeastern Hokkaido, Japan. *Proc. Japan-China Symposium on Landslide and Debris Flows*, Tokyo, Japan, 69-73.

Magaritz, M. and Luzier, J. (1985): Water-rock interactions and seawater- freshwater mixing effects in the coastal dunes aquifer, Coos, Bay, Oregon. *Geochim, Cosmochim. Acta.*, 49, 2515-2525.

Matsukura, Y. and Mizuuno, K. (1986): The influence of weathering on the geotechnical properties and slope angles of mudstone in the Mineoka earthslide area, Japan. *Earth Surface Processes and Landforms*, 11, 263-273.

Matsuo, S. (1957): A study of the effect of cation exchange on the stability of slopes. *Proc. 4th Int. Conf. SMFE.*, 2, 330-333.

Matsuo, S. and Tomita, T. (1970a): The effect of ion exchange on the stability of earth slope (in Japanese). *Materials*, 205, 53-58.

Matsuo, S. and Tomita, T. (1970b): The physicochemical properties of landslide clays and their control. *Proc. 5th Japanese Conf. on Soil Mechanics and Foundation*, 413.

Matsuo, S. Kamon, M., Kamimura, K. and Sasaki, K. (1979): Physicochemical properties of Tertiary type landslide. *Proc. 6th Asian Regional Conf. on SMFE.*, 1, 22-32,

Mitsuno, S. (1985): Subsurface geology (in Japanese). *Geomorphological Land Classification*, National Land Agency, Ed., 18-22.

Miura, K. (1987): Weathering of the plutonic rocks as seen from bore core samples in Sanin district (in Japanese). *Mem. Fac. Educ., Shimane University*, 21, 1-70.

Moore, D. M. and Hower, J. (1986): Ordered interstratification of dehydrated and hydrated Na-smectite. *Clays and Clay Minerals*, 34, 379-384.

Moore, R. (1985): The chemical status of mudslides and its bearing on remedial and preventive measures. *Proc. Symp. on Landslides in the South Wales Coalfield*, Morgan, C. S. Ed., The Polytechnic of Wales, Pontyprid, 122-123.

Moore, R. (1991): The chemical and mineralogical controls upon residual strength of pure and natural clays. *Geotechnique*, 41, 35-47.

Muller-Vonmoos, M. and Loken, T. (1989): *Applied Clay Sci.*, 4, 125-141.

Nakamori, K. and Yang, P. (1991): The method of measuring residual strength of landslide clay (in Japanese with English abstract). *Jour. Japan Landslide Soc.*, 106, 27-32.

Natural Resources Section, Agricultural Structure Improvement Bureau, the Ministry of Agriculture and Forestry, (1973): Landslides of Japan.

Nishida, S. and Tsushimoto, M. (1973): Characteristics of Tertiary formation landslide and its control in Niigada Prefecture (in Japanese). *Soils and Foundations*, 21, 5-13.

Odom, I. E. (1984): Smectite clay minerals - properties and uses. *Phil. Trans. R. Soc. Lond. A.*, 311, 391-409.

Ojanuga, A. G. (1979): Clay minerals of soils in Nigerian Tropical Savanna regions. *Soil Sci. Soc. Am. Jour.*, 43, 1237-1242.

Public Works Office, Okayama Prefecture, (1984): Monden landslide investigation and control.

Public Works Office, Okayama Prefecture, (1990): Monden landslide investigation and control.

Reynolds, R. C. and Johnson, N. M. (1972): Chemical weathering in the temperate glacial environment of the northern Cascade mountains. *Geochim. Cosmochim. Acta.*, 36, 537-554.

Reynolds, S. and Gorsline, D. S. (1992): Clay microfabric of deep-sea, detrital mud(stone)s, California continental borderland. *Jour. Sediment. Petrol.*, 62, 41-53.

Saada, A. S. and Townsend, F. C. (1981): State of the art - Laboratory strength testing of soils. *Laboratory shear strength of soil*, Americal Soc. for Testing and Materials, 7-77.

Shirahata, H., Asahi, H. and Oura, H. (1987): Relationship between rock alteration and landslides in the Noboribetsu district, southwest Hokkaido. *Jour. Japan Soc. Eng. Geol.*, 28, 1-7.

Shuzui, H. (1984): The rock block slide at Hitotsu-Tsubota, Fukushima Prefecture - Especially on the characteristics of clay mineral and quality of groundwater (in Japanese with English abstract). *Jour. Japan Soc. Eng. Geol.*, 25, 23-33.

Shuzui, H. (1986): On the relationship between degree of alteration and landslide (in Japanese with English abstract). *Jour. Japan Landslide Soc.*, 84, 26-30.

Shuzui, H. and Nakamura, F. (1986): For the occurrence and origin of clay layers near sliding surface in Tertiary landslide (in Japanese with English abstract). *Jour. Japan Landslide Soc.*, 85, 20-25.

Shuzui, H. and Kawahara, Y. (1987): On properties of groundwater in Kunini landslide area. *Jour. Japan Landslide Soc.*, 89, 20-29.

Skempton, A. W. (1985): Residual strength of clays in landslides, folded strata and the laboratory. *Geotechnique*, 35, 3-18.

Sobotka, K. (1984): Rheology of materials and engineering structure. Elsevier.

Sridharan, A., Rao, S. M. and Gajarajan, V. S. (1987): Influence of fluoride on the compressibility of montmoriilonites. *Geotechnique*, 37, 197-206.

Tai, Y. (1962): Bentonite deposit and acid clay (in Japanese). *Industrial mineral resources in Chugoku district, Japan*, Committee on development on industrial mineral resources in Chugoku, Ed., 204-212.

Tai, Y. (1972): Post-Miocene crustal movement of the Chugoku district, Japan, with special reference to the structure contour (in Japanese). *Mem. Fac. Gem. Educ. Hiroshima University*, 3, 25-34.

Takeuchi, A. and Takaya, S. (1980): On the composition of clay minerals by X-ray diffraction at B-10 borehole in the Kushibayashi landslide area (in Japanese with English abstract). *Jour. Japan Landslide Soc.*, 61, 17-22.

Tamada, B. (1984): The relation between the constants of shear strength and clay minerals on the landslide surface(in Japanese with English abstract). *Jour. Japan Landslide Soc.*, 82, 7-13.

Tamada, B., Fukuda, J. and Okinaga, (1986): The reaction characteristics of piezonmeter sets on the landslide surface (in Japanese). *Geotech. Rep. Kansai University of Technology*, 2, 1-12.

Tamada, B. and Fukuda, J. (1989): The variation of pore water pressure on the slip surface due to seepage of rain (in Japanese with English abstract). *Jour. Japan Landslide Soc.*, 99, 19-27.

Tamada, B. and Fukuda, J. (1991): Relation between formative process of landslide surface and the clay mineral (in Japanese with English abstract). *Jour. Japan Landslide Soc.*, 107, 25-32.

Tanaka, S. (1991): Quantitative determination of clay minerals in landslide clays (in Japanese). *Proc. 30th Japanese Conf. on Landslide*, 89-90.

Terzaghi, K. (1950): Mechanism of landslides. *Geol. Soc. Am.*, Berkey Volume, New York, 83-124.

Vear, A. and Curtis, C. (1981): A quantitative evaluation of pyrite weathering. *Earth Surface Processes and Landforms*, 6, 191-198.

Veder, C. (1981): Landslides and their stabilization. Springer-Verlag, New York, Wien, 7-18.

Wada, K. (1981): Cation- and anion-exchange capacity measurements for clays (in Japanese). *Jour. Clay Sci. Japan*, 21, 160-163.

Watanabe, T. and Sato, T. (1988): Expansion characteristics of montmorillonite and saponite under various relative humidity conditions. *Clay Sci.*, 7, 129-138.

Yamada, Y. (1989): Experimental study on the relationship between soil structure and consolidation phenomena (in Japanese with English abstract). *Soils and Foundations*, 29, 173-182.

Yamanoi, T., Ishiguro, S., Fuse, H. and Kanda, A. (1974): The landslide of Niigata Prefecture and its environment (in Japanese). *Jour. Japan Landslide Soc.*, 38, 3-14.

Yang, p., Nakamori, K. and Sokobiki, H. (1993): Prediction of the creeping landslide deformation. *Proc. 7th Int. Conf. and Field Workshop on Landslide*, Novosad, S. and Wagner, P., Eds., Czechslovak, 191-197.

Yong, R. N. (1971): Soil technology and stabilization. *Gen. Rep. Sess. 5, Asian Reg. Conf. SMFE*, Bangkok, 2, 111-124.

Yong, R. N. and Warkentin, B. P. (1975): Soil properties and behaviour. Elsevier, Amsterdam, 21-1000.

Zaruba, Q. and Mencl, V. (1982): Landslides and their control. Elsevier, New york, and Academia, Prague, 31-53.

Pucai YANG
Institute of Geology and Mineralogy,
Faculty of Science, Hiroshima University,
Higashihiroshima 724, Japan.

Explanation of Plate

Plate 1. SEM micrographs of undisturbed samples from the landslide profile A63-2. A: Showing skeletal-matrix texture (3.0 m deep), B: Enlarged view of cluster dominated by EF particle contacts, C: Showing skeletal-matrix texture (4.5 m deep), D: A coating of fine-granule materials on the surface of particle (4.5 m deep).

Plate 2. SEM micrographs of the landslide clays (5.0 m from the landslide profile A63-2). A: Showing slideing cast and slickenslide (surface parallel to the slip zone), B, C and D: Showing highly oriented parallel FF particle contact texture (surface parallel to the slip zone).

Plate 3. SEM micrographs of typical flocculent texture (5.5 m from the landslide profile A63-2). A: Showing vertical section of parallel clay particles, B: Enlarged view of flaky clays.

Plate 4. SEM micrographs showing flocculent texture with randomly oriented clusters (A and B: from the landslide profile A63-2 at 6.0 m and 11.0 m depths, respectively).

Plate 5. SEM micrographs showing porous skeletal-matrix texture (3.0 m deep from the landslide profile B63-4). A: Surface parallel to the slip zone, B: Enlarged view of skeletal-matrix texture.

Plate 6. SEM micrpgraphs of undisturbed samples from the landslide profile B63-4 (5.0 m deep). A: Showing dominant cluster contact texture (surface parallel to the slip zone), B: Enlarged view of cluster contact texture.

Plate 7. SEM micrographs of the landslide clays from the landslide profile B63-4 (5.5 m deep). A: Showing a strongly parallel particle orientation with nearly perfect FF contact (surface parallel to the slip zone), B: Showing slickenside parallel to the slip zone, C: Showing oriented cluster contact texture (surface parallel to the slip zone), D: Showing randomly oriented cluster contact texture (surface normal to the slip zone).

Plate 8. SEM micrographs showing flocculent texture (A and B taken from the landslide profile B63-4 at 9.0 m and 12.0 m deep, respectively).

Plate 9. SEM micrographs of sheared samples. A and B: Showing randomly oriented cluster contact texture (surface normal to sheared zone), C: Sheared zone showing a strongly oriented cluster contact texture, D: Sheared zone showing a highly parallel orientation with perfect FF contact.

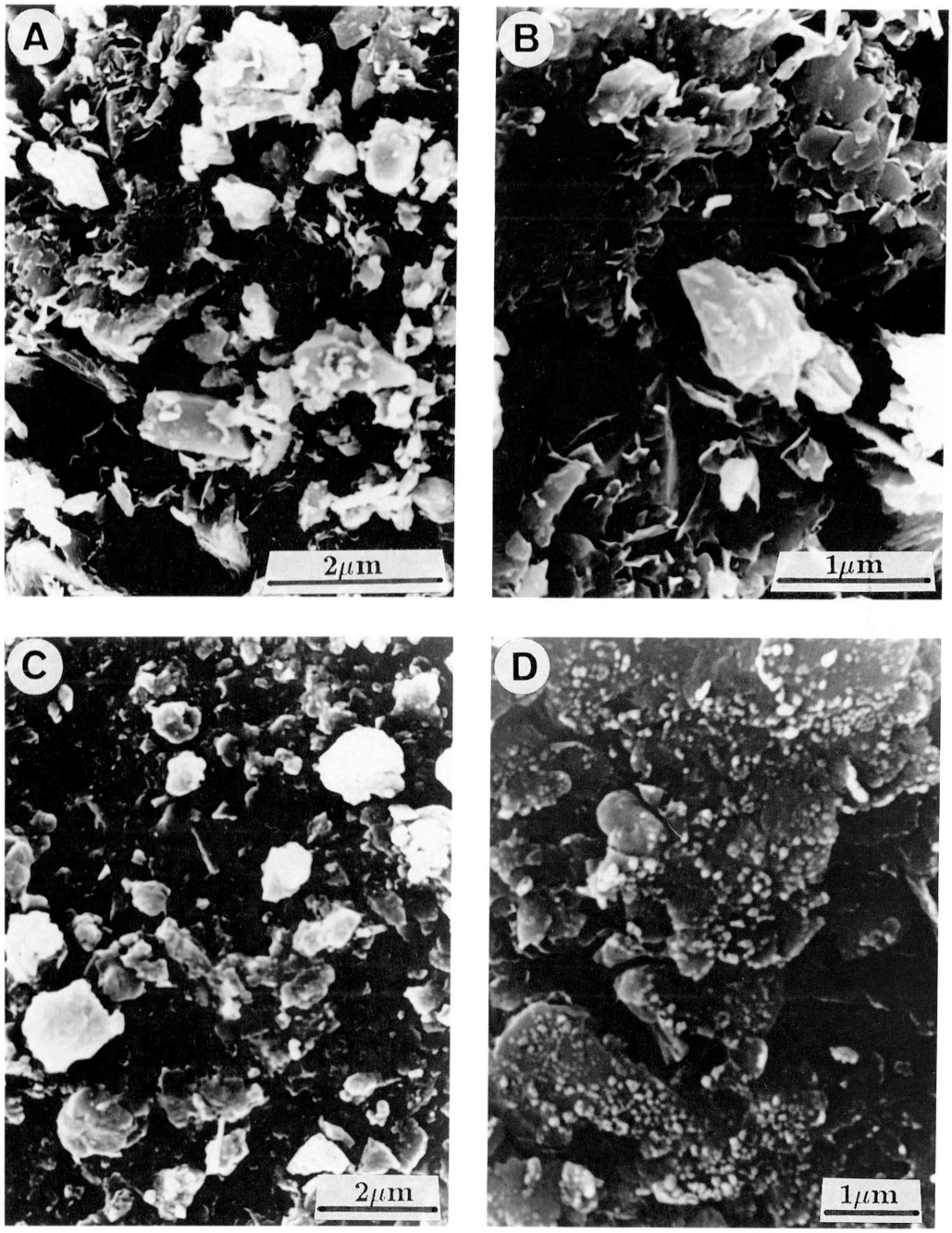

Plate 1

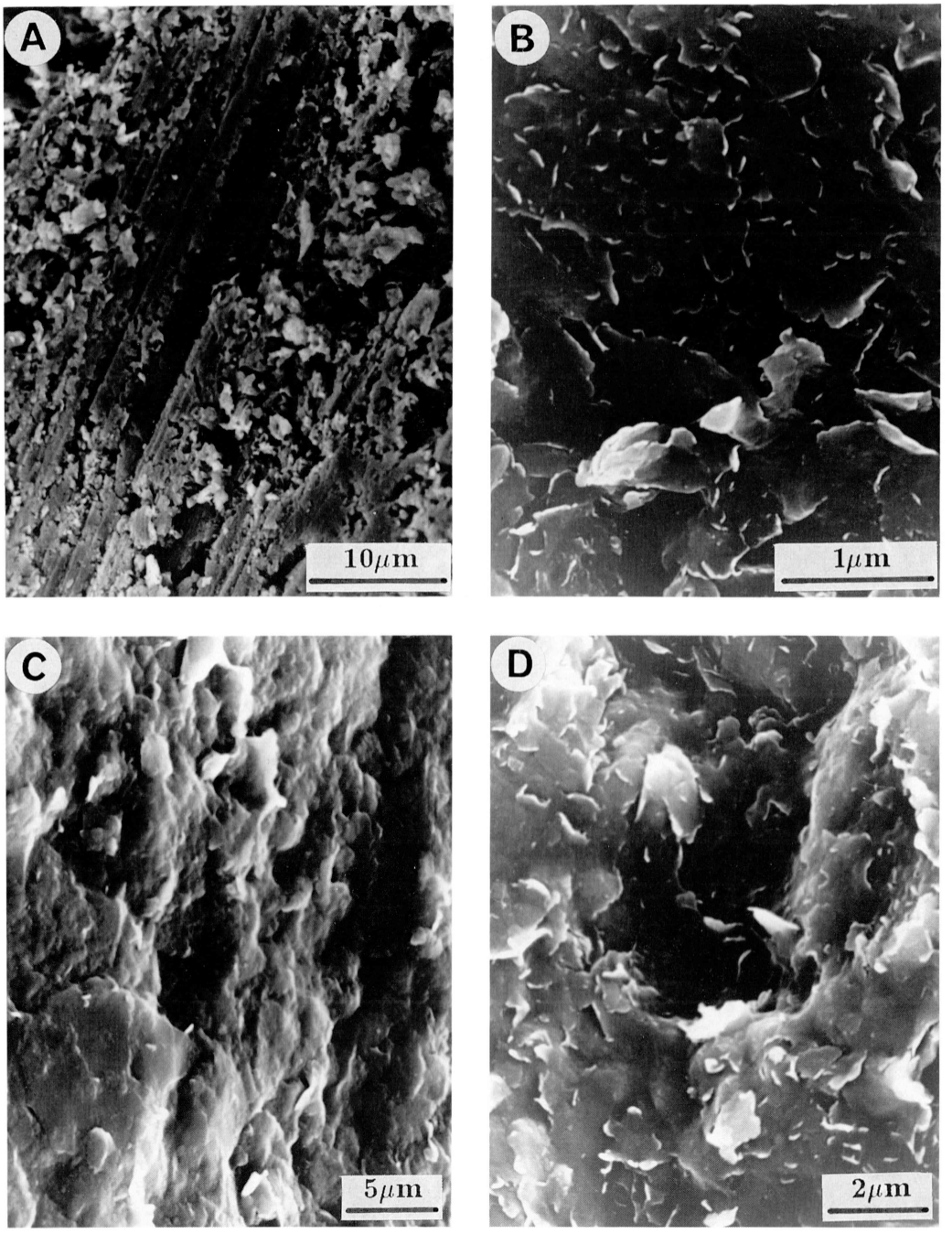

Plate 2

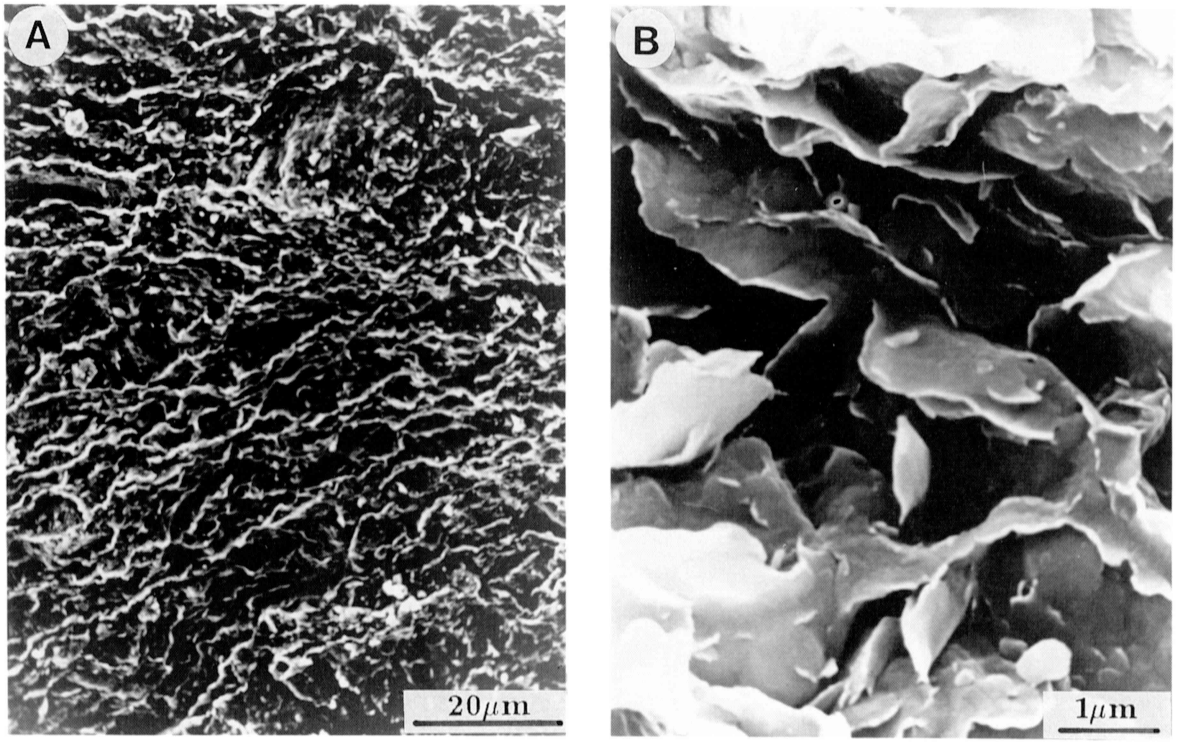

Plate 3

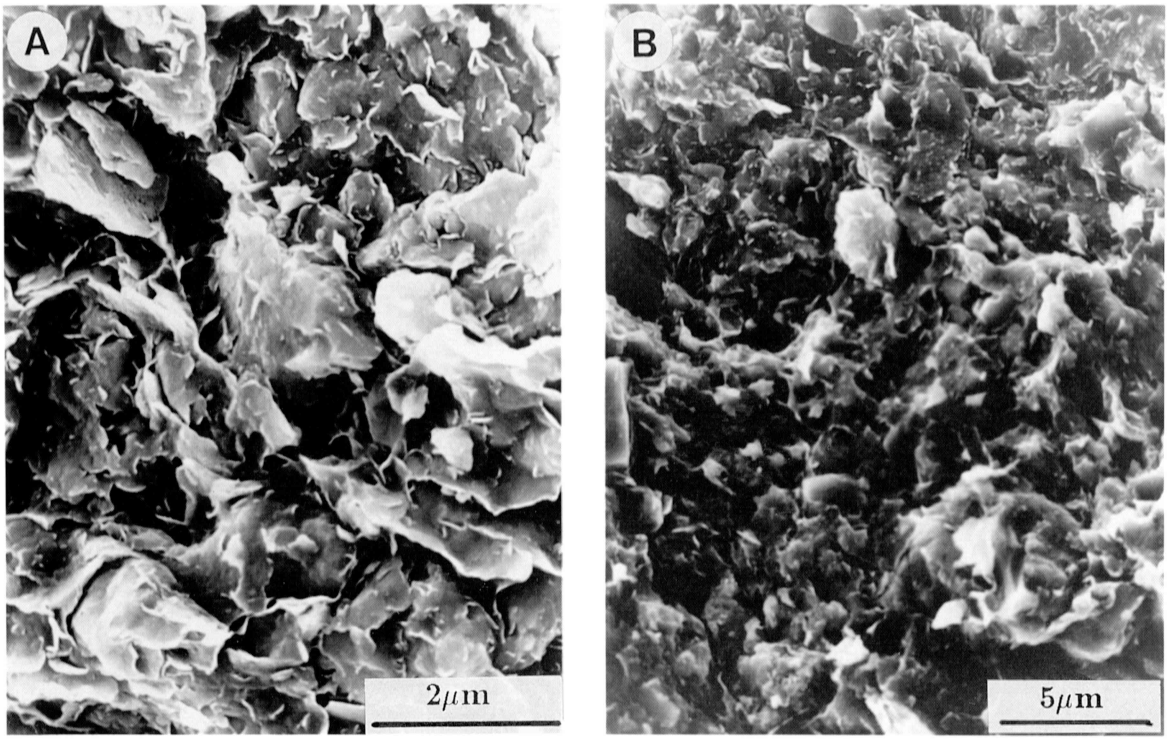

Plate 4

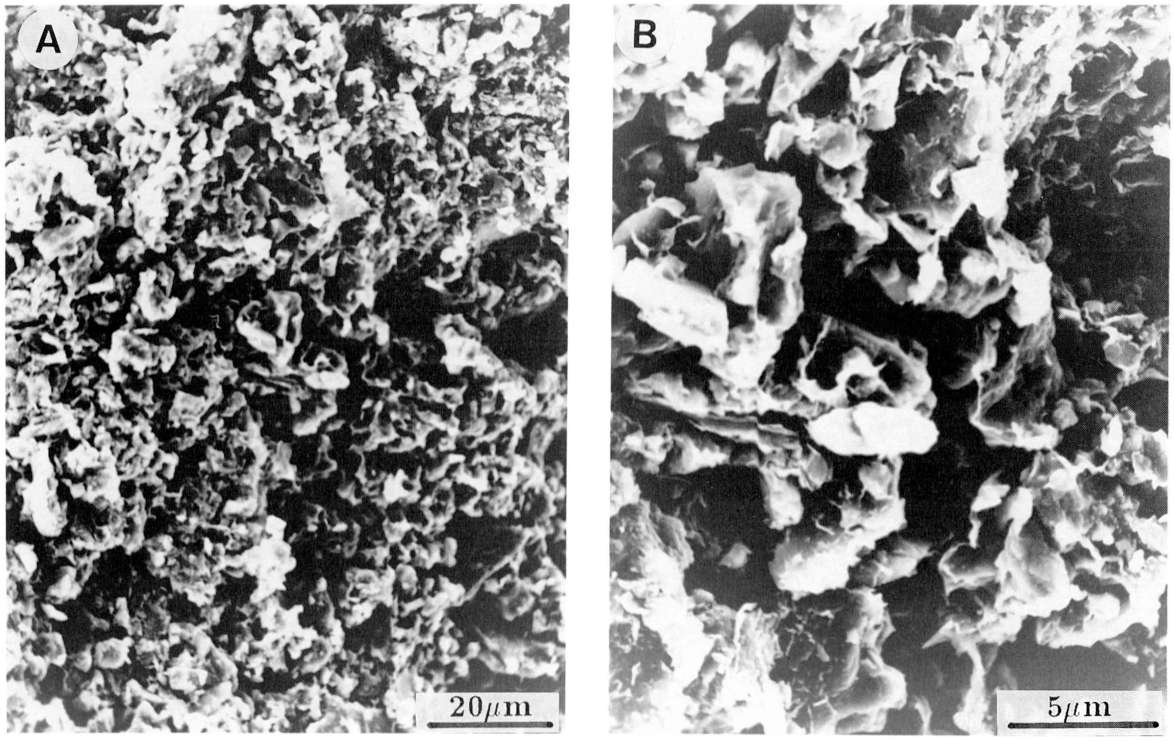

Plate 5

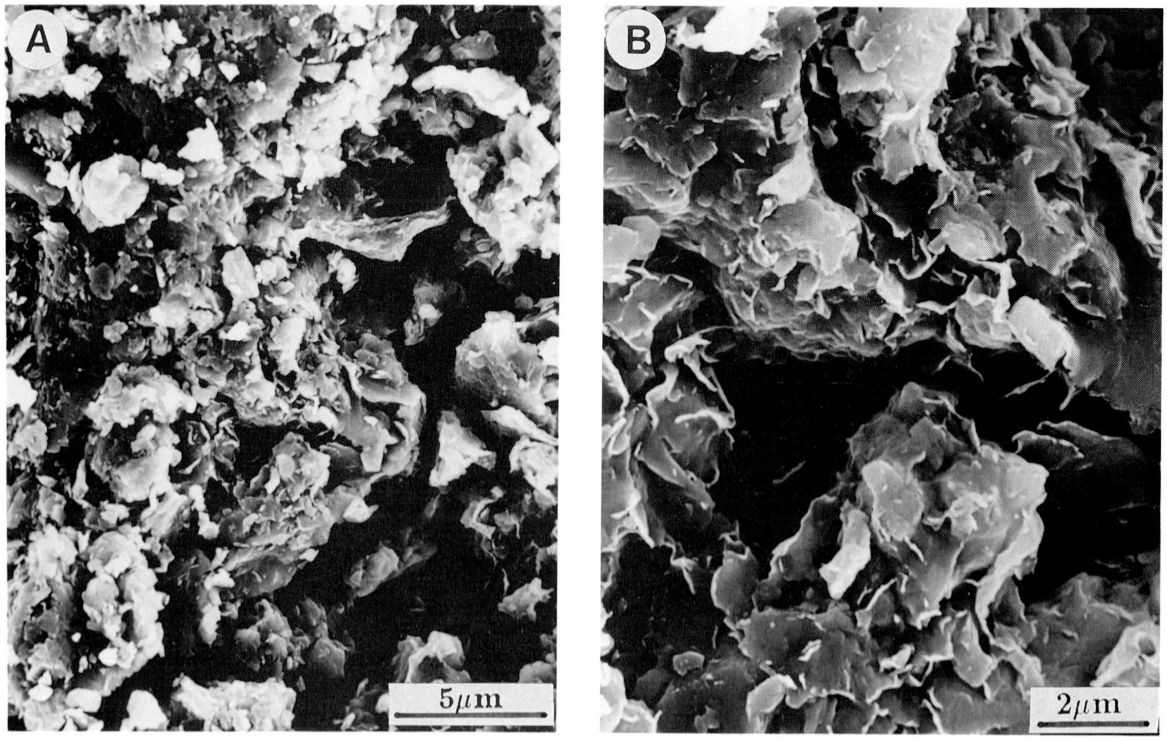

Plate 6

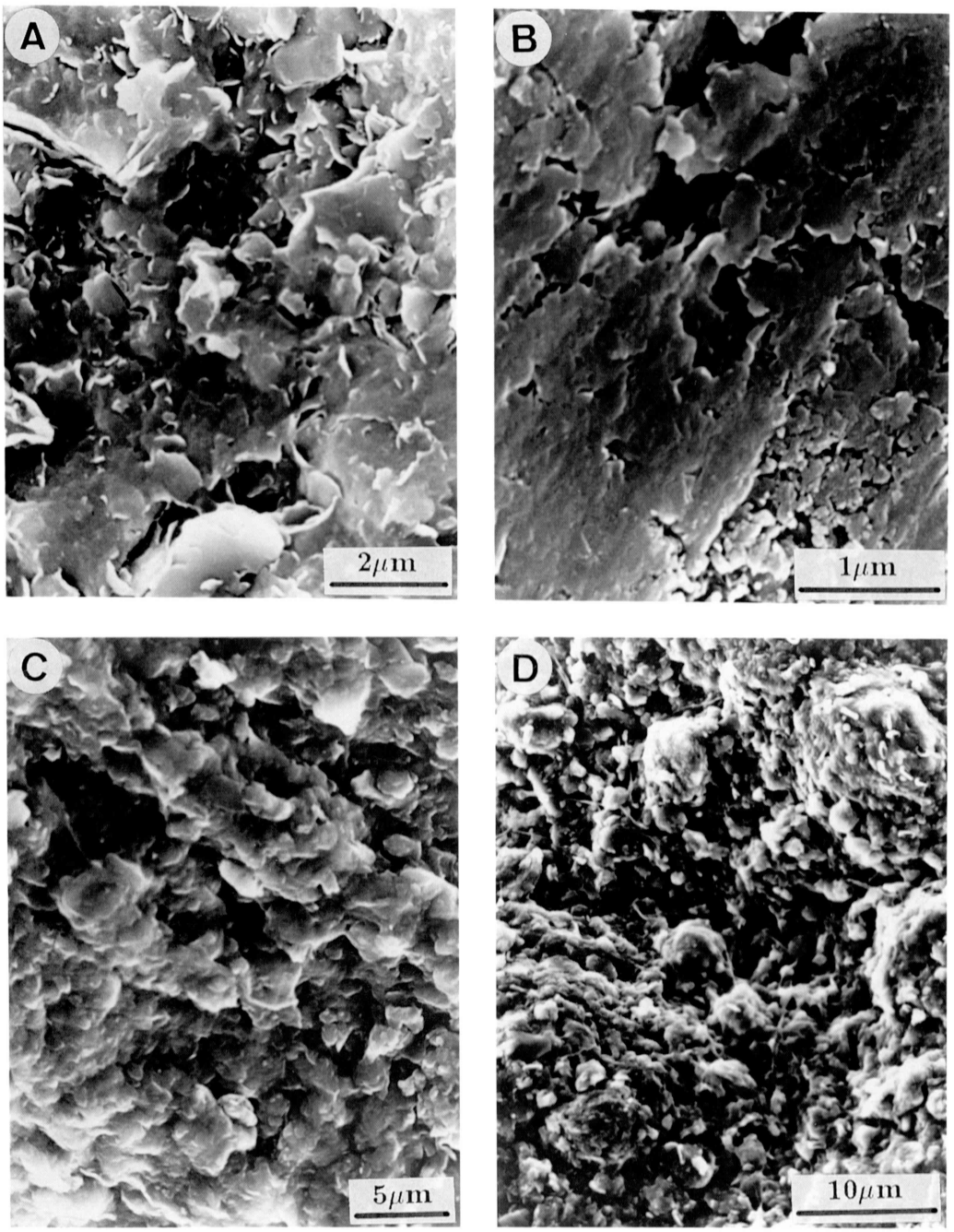

Plate 7

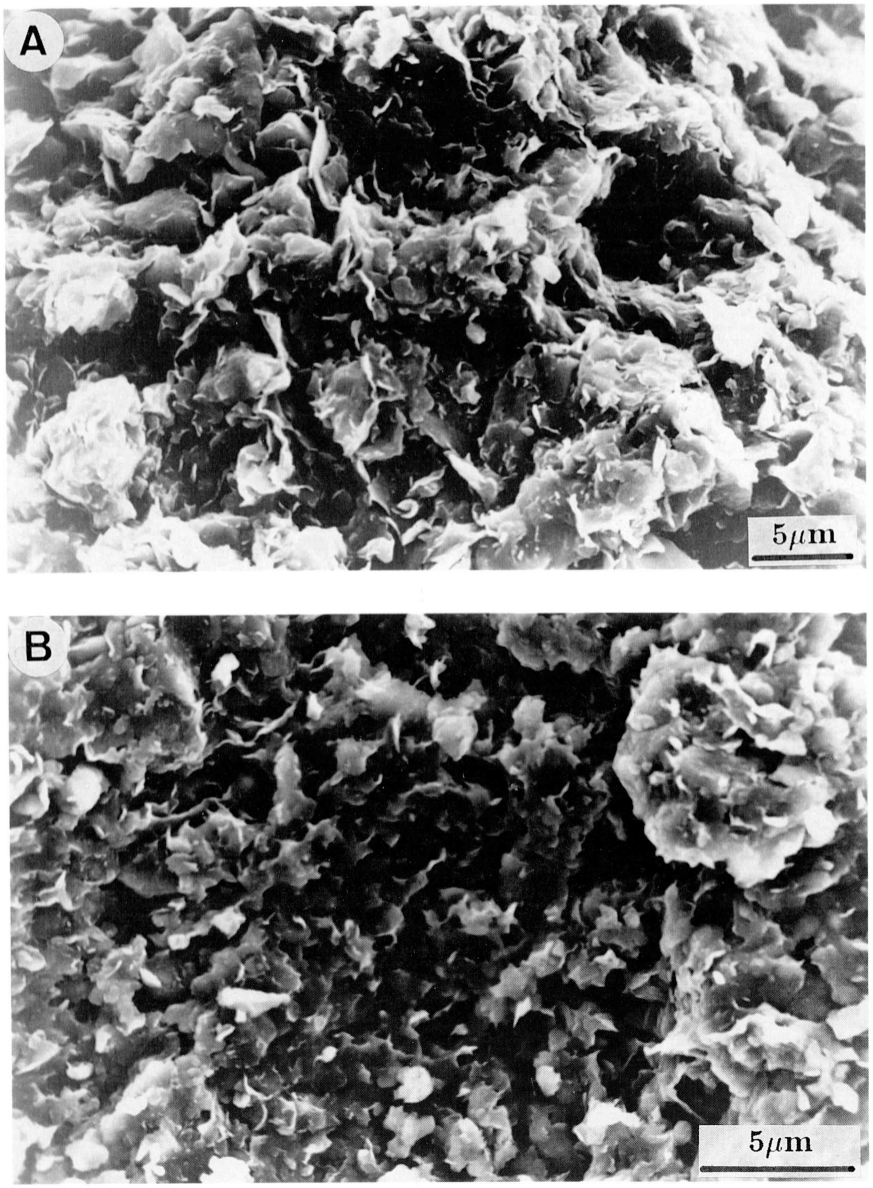

Plate 8

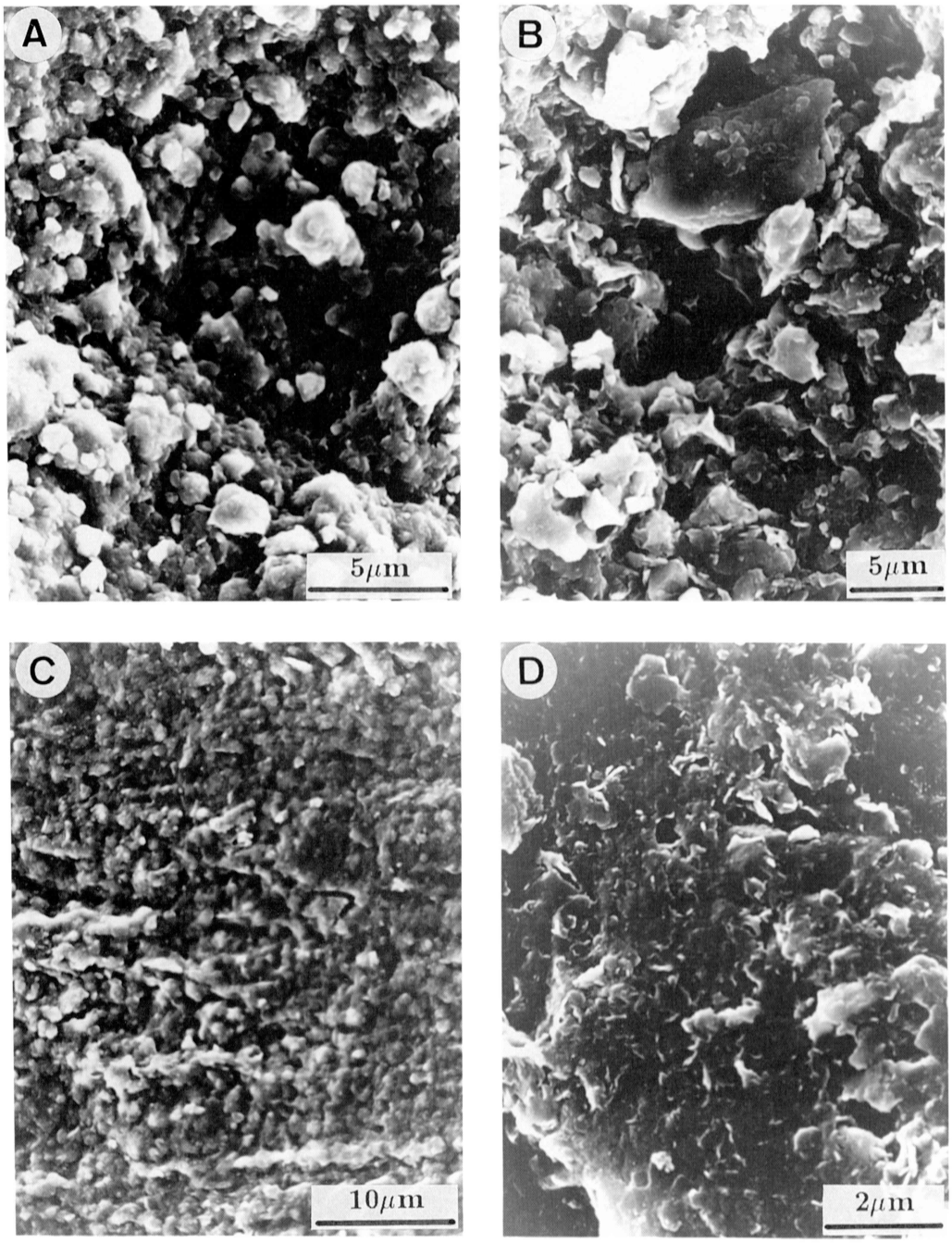

Plate 9